Order Number 1349458

An approximate method for determining the frequency dependent current distribution in a ground plane

Mehra, Arun, M.S.

The University of Arizona, 1992

U·M·I
300 N. Zeeb Rd.
Ann Arbor, MI 48106

AN APPROXIMATE METHOD FOR DETERMINING THE FREQUENCY DEPENDENT CURRENT DISTRIBUTION IN A GROUND PLANE

by

Arun Mehra

A Thesis Submitted to the Faculty of the

DEPARTMENT OF ELECTRICAL AND COMPUTER ENGINEERING

In Partial Fulfillment of the Requirements
For the Degree of

MASTER OF SCIENCE
WITH A MAJOR IN ELECTRICAL ENGINEERING

In the Graduate College

THE UNIVERSITY OF ARIZONA

1992

STATEMENT BY AUTHOR

This thesis has been submitted in partial fulfillment of requirements for an advanced degree at The University of Arizona and is deposited in the University Library to be made available to borrowers under rules of the Library.

Brief quotations from this thesis are allowable without special permission, provided that accurate acknowledgement of source is made. Requests for permission for extended quotation from or reproduction of this manuscript in whole or in part may be granted by the head of the major department or the Dean of the Graduate College when in his or her judgment the proposed use of this material is in the interests of scholarship. In all other instances, however, permission must be obtained from the author.

SIGNED: _____

APPROVAL BY THESIS DIRECTOR

This thesis has been approved on the date shown below:

_____ _____

Andreas Cangellaris
Professor of
Electrical and Computer Engineering

8/21/92
Date

ACKNOWLEDGEMENTS

I would like to thank Dr. John L. Prince and Dr. Andreas Cangellaris for their constructive review of my thesis and financial support during this period.

I would also like to express my sincere gratitude to Dr. Andreas Cangellaris for his guidance and immeasurable support. I am especially grateful to him for his encouragement throughout the course of my work.

I would like to thank Dr. R. Schrimpf for taking the time to participate on my thesis committee.

Finally, I wish to give special thanks to Ramesh Senthinathan for his help in offering valuable suggestions and general support.

TABLE OF CONTENTS

LIST OF FIGURES

ABSTRACT

This MS thesis proposes a methodology to compute the frequency dependent current distribution for a ground plane with the ultimate aim of utilizing this current distribution to compute the plane parasitics. The need to understand the current distribution in a ground plane is becoming critical as speed and density increases in VLSI devices.

An iterative finite differencing technique is utilized to solve the two dimensional diffusion equation for the current distribution on the plane. Starting with an initial DC current density over the entire plane grid, the frequency dependent current density is obtained by imposing the necessary boundary conditions and allowing the current to redistribute itself over the plane. The initial DC current density is obtained from UALGRL (a DC current distribution calculator for a ground plane).

An iterative procedure based on simultaneous over relaxation is employed to get faster convergence. This method takes into account the presence of sources, sinks and holes on the plane. Finally the plane parasitics are computed using integral methods and energy considerations.

CHAPTER 1

1.1 Introduction to Electronic Packaging

A package is defined as a group or a number of things, boxed and offered as a unit. Electronic packages contain many electrical circuit components - millions in case of a large computer - notably resistors, capacitors, diodes and transistors. To form circuits these components need interconnections. Individual circuits must also be connected with each other to form functional units. Mechanical support and protection are required for those units. To function, electrical circuits need to be supplied with electrical energy which is consumed and transformed into thermal energy. Because all circuits operate best within a limited temperature range, packaging must offer an adequate means for removal of heat. Thus we can sum up the four main functions of an electrical package:

- Power Distribution.
- Signal Distribution.
- Heat Dissipation.
- Circuit Protection.

A package must also be manufacturable at an affordable cost and repairs be easy and inexpensive.

One reason why packaging has become so important is the imperative to make the central elements of a computing system exceedingly compact. Improvements in the design and fabrication of microelectronic devices have greatly increased the number of logic functions that can be put on a chip as

well as the speed at which arithmetic operations are performed. In many high speed data processing units packaging technology is the factor that determines or limits performance, cost and reliability. Today, a major source of delay in the central processing unit of many computers is the time needed for a signal to pass from one chip to another. In order to reduce the delay the chips must be put closer together. Fitting many chips, each with many terminals, into a small volume challenges packaging technology in many ways. The reasons for the shortcomings of present packaging technology to implement high performance systems at low cost are well known. First, chip to chip interconnectionc are too long, the dielectric constant of the propagating medium too high and signal delay too long. Some of the electrical problems include impedance mismatch, crosstalk, signal reflection and ground plane noise.

An entirely new packaging technology that is gaining importance in the semiconductor industry today is the MCM (Multi Chip Module) technology. This technology offers considerable advantages over the old approach, though at a much higher cost and manufacturing complexity.

1.2 Importance of Studying the Ground Plane

Having understood the functions of an Electronic Package, let us now look into the utility of a ground plane in a package and the need to analyse it. In a high performance package, the wire that carries a signal cannot be considered a

simple conductor but instead must be treated as a transmission line. This is necessary because, propagation delays are important and the signal needs to be represented as a wave propagating along the transmission line. The basic method of controlling the characteristics of transmission lines is to separate layers of signal wires with conductive sheets called voltage reference planes.

These reference planes distribute power to the chip (power plane) and also provide a path for return currents (ground plane). Ideally each plane is assumed to be at a uniform electric potential, either zero volts (ground voltage) or one of the supply voltages needed by the chip. A signal line encased in an insulating medium and sandwiched between two such planes makes a transmission line whose properties can be calculated. The planes [5] give the line a uniform and well defined impedance and also inhibit crosstalk between lines in adjacent layers.

One of the most important problem in today's VLSI packages that warrants a comprehensive analysis of the ground plane is "switching noise", also called ground noise or ground bounce. The ground and power noise in VLSI CMOS devices is becoming a critical factor as speeds and density increase. Ground bounce [13] is the variation of the chip ground voltage relative to the external ground and can occur when many drivers switch simultaneously. The varying current that these drivers conduct generates a voltage across the parasitic inductance of the package consisting of the bonding wire, ground plane and package pin.

For a chip at the fast processing extreme, the output buffers will transfer charge in a short period of time. This implies short rise/fall times and a large voltage spike will be developed across the parasitic inductance. For a chip at the slow processing extreme, the rise/fall time is increased generating less ground bounce. These two extremes determine output buffer design.

A significant amount of switching noise [7] may be generated in the ground/power plane (VSS/VDD Plane) and in the internal VDD/VSS buses. Unless these noise fluctuations can be controlled, simultaneous switching noise can degrade or even limit the system performance. One method to reduce the simultaneous noise is to increase the number of VDD/VSS connections. It is thus essential to calculate the package VDD/VSS inductance to accurately define a total effective inductance in power/ground noise calculations.

In the past, it was assumed that all VDD/VSS connections are identical and therefore the effective inductance seen by the driver was L/p, where "L" is the inductance for each identical connection (bonding wire+plane+package) and "p" is the number of connections. This is only true if all connections are symmetrical and mutual inductances negligible.

As the bond pad to pad and package pin to pin pitch decreases and/or if the connections are non-symmetrical one needs to extract the exact parasitics from the VDD/VSS planes to have some meaningful switching noise values.

The figure below shows the parasitics involved in modeling switching noise problems:

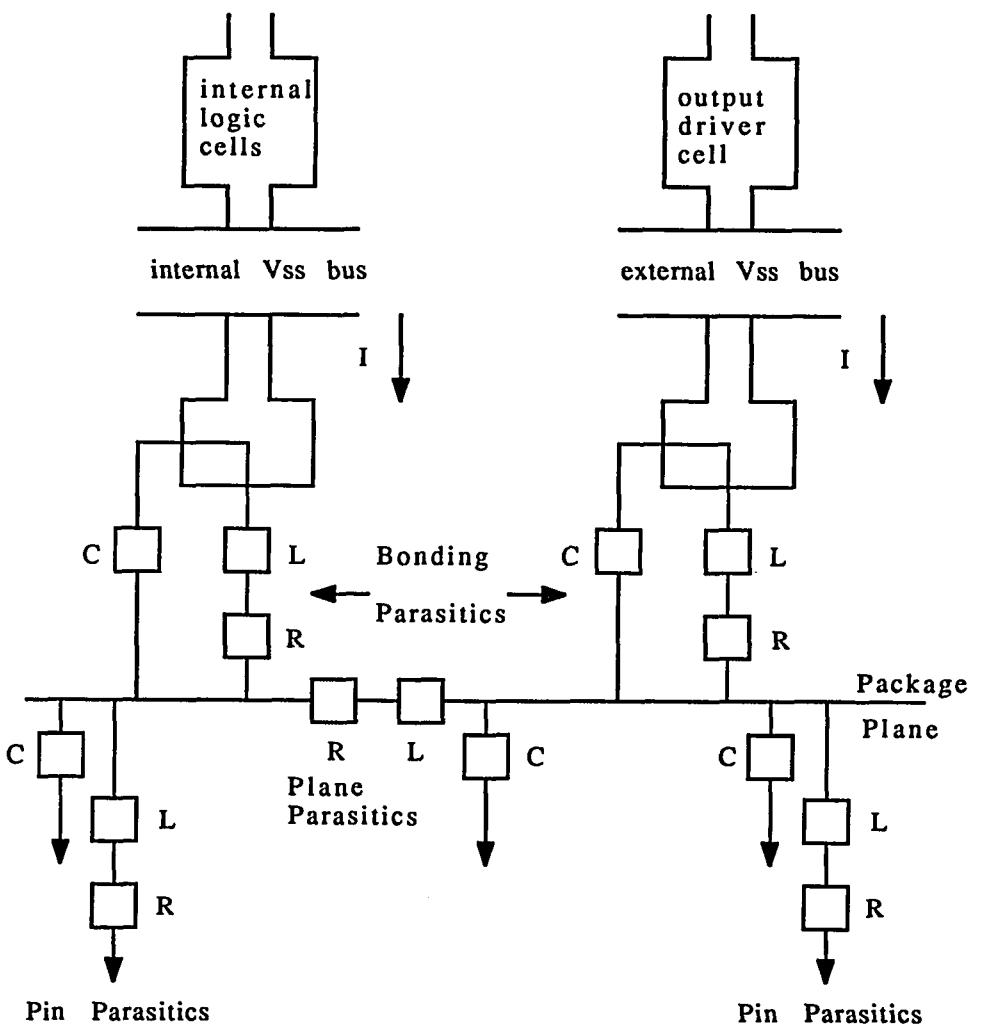

FIGURE 1: Switching Noise Computation Model [12]

From the previous discussion, the criticality of understanding the current distribution among the various pins connected to the power and ground plane and extracting the associated plane parasitics for the prediction of the inductive noise and DC drop need not be emphasized. Equal current distribution from the device to the package pins insures maximum reduction of effective inductance as well as resistance in the power and ground loop [6]. The modeling of the current density is generally difficult due to the boundary conditions imposed by complicated plane geometries and the presence of holes and cuts.

Having optimized the current distribution through each pin we can effectively place them in the package and can also improve the plane inductance by varying the number and placement of source points entering the plane. In the past, it was assumed that simultaneous switching noise created by CMOS outputs was directly proportional to the number of outputs switching simultaneously. However, recent studies indicate that CMOS circuits exhibit sublinear behaviour due to negative feedback influence of ground noise as a function of number of outputs switching simultaneously [12]. All these reasons form the basis for an extensive study and analysis of the ground plane.

In a multilayer VLSI package, the correct use of ground and voltage reference plane leads to a reduction of the noise coupling and crosstalk that occur during signal switching. This problem also entails evaluating a ground current magnitude distribution due to a current source and sink pair [10]

and computing the current induced on a ground plane due to a signal line above it.

Having enumerated all the reasons to analyse power/ground planes in today's multi-layered VLSI packages, let us now look into one methodology for developing the current distribution in a ground plane. A similar approach can be used for a power plane.

1.3 Organisation of Thesis

The second chapter discusses the theoretical development of the current model starting with the DC current distribution. This chapter includes the detailed specifications regarding the iterative technique used to compute the current, the interpolation of the potential values obtained from UALGRL in order to get the initial current values and the boundary conditions imposed on the plate.

All these topics form the basis of the entire thesis and are critical to the phase involving algorithm development and implementation. This chapter concludes with the methodology used to compute the resistance and inductance of a plane given the current distribution at discrete points on the plane.

Chapter 3 focuses on the examples used to validate the theory and code. The verification of the entire model is done with results obtained through program execution. A manual sheet also provides the necessary guidance to run the program and how to choose the values of the variables involved. The results are then presented for each example.

The write-up terminates with a discussion of the performance of the proposed model and further developments needed for its completion. The appendix section includes sample input files and talks about program execution.

CHAPTER 2

2.1 UALGRL Model Definition

UALGRL is a Fortran 77 finite element program developed at the Center for Electronic Packaging, University of Arizona [4]. The program calculates the potential and current distributions in rectangular power and ground planes which may contain rectangular perforations. The user specifies the potential at a number of points (sources or sinks) in the interior of the plane. In addition, the user also specifies the number, size and location of the perforations, the dimensions of the plane itself and its thickness and conductivity. The program finally calculates the current entering or leaving each source or sink point and the effective DC resistance and partial self-inductance of the plane for the given source sink configuration.

From a packaging point of view, the sources can represent locations where the current is drawn into the plane (connections to the power supply) and the sinks can represent locations where current is leaving the plane (i.e., vias connecting the plane to ground pads on the chip). The hole can represent plated through holes which provide ways for connections from layers above to layers below the plane, as is often the case in multi-layer ceramic packages.

The actual potential on sources/sinks does not have any effect on the values of R and L as long as all sources have the same potential and all the sinks are at

the same potential. This is because the distribution of the currents will remain the same and only the magnitude of the currents will change in proportion to the potential. On the other hand, if sources are not kept at the same potential, the inductance and resistance will be effected because the current distributions on the plane will change. Some of the features of this program are as follows:

1) Flexible input/output processing.
2) User friendly mesh generation.
3) Sources and sinks can lie on the edge of the plane.
4) The plane can be divided into regions of different conductivity.

Figure 2, below, shows some of the typical geometries that can be modeled efficiently using UALGRL.

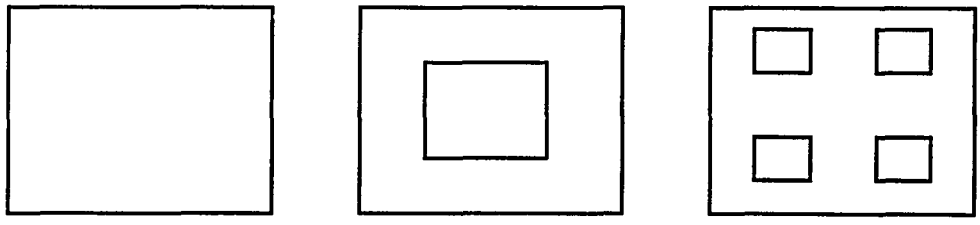

FIGURE 2: Typical geometries in UALGRL

Geometries that cannot be modeled exactly by UALGRL are shown in Figure 3.

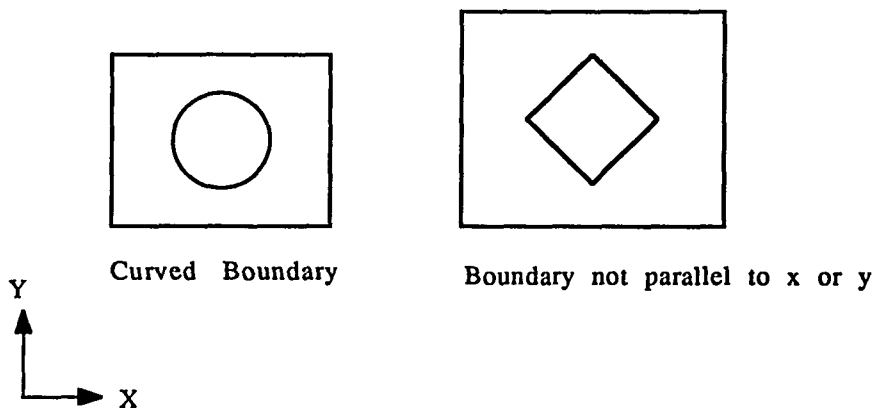

FIGURE 3: Geometries that cannot be modeled using UALGRL

Planes can be divided into a maximum of 100 rectangular regions characterized by different values of conductivity. However, as the number of elements increases, the run time and memory requirements also increase. Doubling the number of elements results in the execution time approaching the square of its original value. A good technique is to start with coarse discretization and make it finer and finer while observing the effects on the results.

Let us now see how the mathematical formulation is developed to compute the resistance and inductance of the plane.

Let 'v' be the volume the conducting plane occupies. Inside v, the electric field is given by:

$$\bar{E} = -\nabla\phi - j\omega\,\bar{A} \qquad \text{— (1)}$$

where ϕ denotes the electric potential and ω is the radian frequency. The current density in v is obtained by applying Ohm's law to (1):

$$J = -\sigma\nabla\phi - j\omega\sigma\,\bar{A} \qquad \text{— (2)}$$

where σ is the conductivity of the plane which is assumed to be much larger than $\omega\varepsilon_0$ (so that displacement currents in the plane are negligible). Here one should use typical values for σ and state of the art values of ω to examine wether this assumption is realistic. In the quasi-static limit where magnetic diffusion effects are negligible, equation (2) becomes

$$\bar{J} = -\sigma\nabla\phi \qquad \text{— (3)}$$

Taking the divergence of (3) and recognizing that $\nabla .\ \bar{J} = 0$ inside a good conductor, we obtain Laplace's equation:

$$\nabla^2\phi = 0 \qquad \text{— (4)}$$

The appropriate boundary condition for quasi-static current flow is:

$$\partial\phi / \partial n = 0 \qquad \text{— (5)}$$

on s, where n is the outward unit normal to v. The physical meaning of (5) is that there is no current flow out of the plane. The Finite Element Method is used to solve the boundary value problem defined by (4) and (5) along with a Dirichlet boundary condition enforced at nodes corresponding to sources and sinks. Volume v is a rectangular plate of thickness t where the current is assumed to be uniform in the direction of t. Thus the resulting FEM formulation is two dimensional where bi-linear shape functions are used in conjuction with four node isoparametric elements.

Equation (3) is used to determine the current distribution throughout the discretized v. The current leaving each source (or sink) is calculated from:

$$I = t\int_c \bar{J} \cdot n \; dl \qquad \text{--- (6)}$$

where c is the contour shown in Figure 4, and n is the outward unit normal on c.

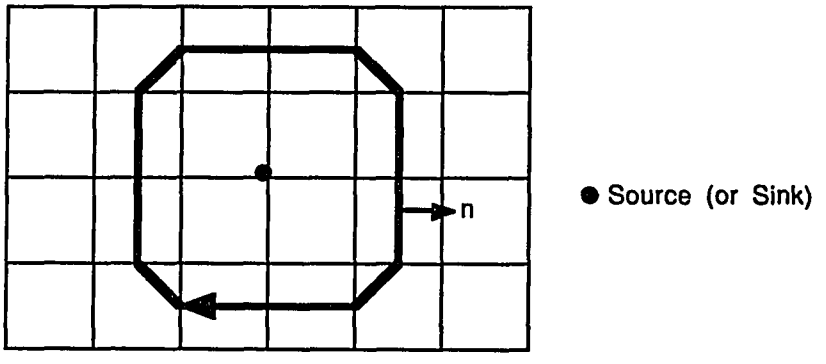

FIGURE 4: Integration area in UALGRL

The contour c was chosen because the variation of J within elements sharing a source point is very large due to the singular behavior of the source. Once the current is determined, the resistance follows from:

$$\frac{1}{\sigma}\int_v (\bar{J}^* \cdot \bar{J})\, dv = R|I_{tot}|^2$$

where I_{tot} is the sum of the currents from the source points. Again, under the quasi-static assumption, the vector magnetic potential, $\bar{A}$, is obtained as

$$\bar{A} = \mu\int_v \bar{J}(\bar{r}')\, G(\bar{r}/\bar{r}')\, dv'$$

where μ is the permeability of v and $G(\bar{r}/\bar{r}')$ is the free space Green's function.

$$G(\bar{r}/\bar{r}') = \frac{1}{4\pi} \frac{1}{|\bar{r}-\bar{r}'|}$$

The effective partial inductance of the ground plane is obtained from:

$$\text{Re}\{\int_v \bar{J}^* \cdot \bar{A}\, dv\} = L|I_{tot}|^2$$

Thus we get the resistance and inductance of the plane. The plane inductance and resistance decrease as the number of sources or sinks per side increase. However, this happens till a certain point, after which any further increase in the number of sources or sinks per side decreases the plane inductance and resistance only slightly.Having explained this computation for the D.C. case, let us now try to develop a methodology for the frequency dependent current distribution in a ground plane, where the magnetic diffusion effects are taken into account.

2.2 Mathematical Formulation

The frequency dependent current distribution in a ground plane is solved using Maxwell's equations. This is necessary in order to explain the electromagnetic phenomena associated with time harmonic fields. In the study of electromagnetics, we are concerned with the following four vector quantities:

$\bar{E}$: Electric field strength (volts per meter)

$\bar{D}$: Electric flux density (coulombs per square meter)

$\bar{H}$: Magnetic field strength (amperes per meter)

$\bar{B}$: Magnetic flux density (webers per square meter)

These are vectors and are always functions of time and space. The Maxwell equations are:

$$\nabla \times E = -\partial B/\partial t \qquad -- (7)$$

$$\nabla \times H = J + \partial D/\partial t \qquad -- (8)$$

$$\nabla . B = 0$$

$$\nabla . D = \rho_v$$

where J and ρ_v are the sources generating the electromagnetic fields. We also know that for a linear isotropic medium the fluxes are related to the fields in a simple manner,

$$B = \mu H \qquad -- (9)$$

$$D = \varepsilon E \qquad -- (10)$$

where μ is the magnetic permeability and ε is the electric permittivity of the medium. Therefore from (7) and (8), (9) and (10) we have:

$$\nabla \times \bar{E} = -\mu \frac{\partial \bar{H}}{\partial t}$$

$$\nabla \times \bar{H} = \sigma \bar{E} + \varepsilon \frac{\partial \bar{E}}{\partial t}$$

Let us now assume that displacement currents $\varepsilon \frac{\partial \bar{E}}{\partial t}$ are negligble in a good conductor. Therefore, the maxwell's curl become

$$\nabla \times \bar{E} = -\mu \frac{\partial \bar{H}}{\partial t} \qquad \text{— (11)}$$

$$\nabla \times \bar{H} = \sigma \bar{E} \qquad \text{— (12)}$$

Taking the curl of (11) we get:

$$\nabla \times \nabla \times \bar{E} = -\mu \frac{\partial}{\partial t} (\nabla \times \bar{H})$$

Using (12) and the vector identity $\nabla \times \nabla \times \bar{F} = \nabla (\nabla . \bar{F}) - \nabla^2 \bar{F}$ we get,

$$\nabla (\nabla . \bar{E}) - \nabla^2 \bar{E} = -\mu\sigma \frac{\partial}{\partial t} (\bar{E})$$

Inside the good conductor there is no charge accumulation. Thus, $\nabla . \bar{E} = 0$ and the above equation simplifies to

$$\nabla^2 \bar{E} = \mu \sigma \frac{\partial}{\partial t} (\bar{E})$$

Finally using ohm's law $\bar{J} = \sigma \bar{E}$, we obtain

$$\nabla 2 \bar{J} = \mu\sigma \ (\partial \bar{J} / \partial t) \qquad \text{-- (13)}$$

This is the diffusion equation for the current density in a good conductor. For time harmonic fields with time variation $e^{j\omega t}$ the above equation becomes

$$\nabla^2 \bar{J} = j\omega \mu\sigma \bar{J}$$

where $\bar{J}$ is now a complex vector quantity, and f the frequency. For a two dimensional case, we have:

$$\nabla^2 J_x - j\omega \mu\sigma J_x = 0$$

and

$$\nabla^2 J_y - j\omega \mu\sigma J_y = 0$$

The objective is now to solve these two equations over the plane, subject to appropriate boundary conditions to be explained later. Let us now turn to the finite difference technique used to approximate the diffusion equation and eventually obtain its numerical solution.

2.3 The Finite Difference Method

Finite difference methods are used to obtain approximate solutions of partial differential equations (PDE's) over a discretized version of the domain of interest. A brief review of the finite difference technique follows, starting with the nomenclature and fundamental concepts behind the method.

The basic concepts are quite simple. The domain of solution of the given PDE is first discretized by means of a net with a finite number of mesh points. The derivative at each point is then replaced by a finite difference approximation. Alternatively, one can visualize this discretization procedure as the replacement of the solution of the PDE with an interpolating polynomial and the differentiation of this polynomial.

Let us first consider u(x), in which 'u' is a continuous function of the single independent variable 'x'. This is shown in Figure 5 on the next page. We discretize the x domain into a set of points such that:

$u(x_r) \equiv u(rh) \equiv U_r \qquad r = 0, 1, 2 \ldots$

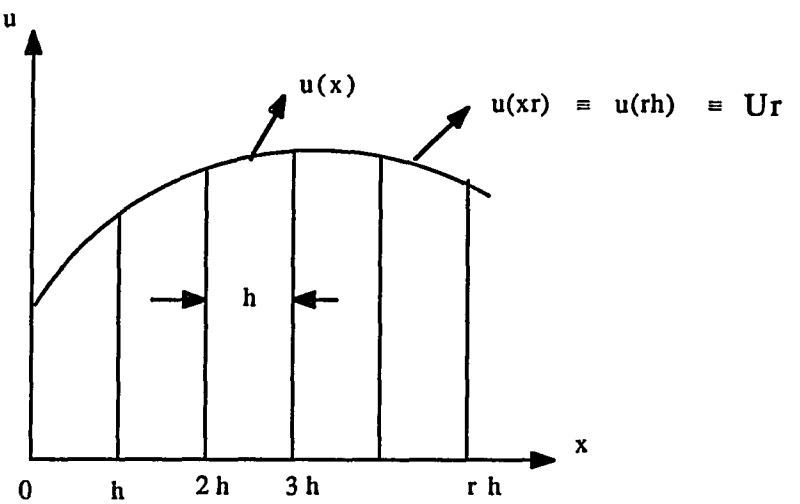

FIGURE 5: Curve illustrating the finite difference method

By replacing the location x_r by rh, the nodal coordinates are specified simply as the product of the integer 'r' and grid spacing 'h'. The integer 'r' denotes the position of the node along the 'x' coordinate relative to a specified datum, usually r = 0 when x = 0.

Now let us consider a function u(x,y). A partial derivative of this function with respect to x implies that y is held constant and vice-versa. In reference to Figure 6 on the next page, we have:

$$\frac{\partial u}{\partial x}_{r,s} \equiv u_x|_{r,s} \cong (U_{r+1,s} - U_{r,s})/\ h + O(h)$$

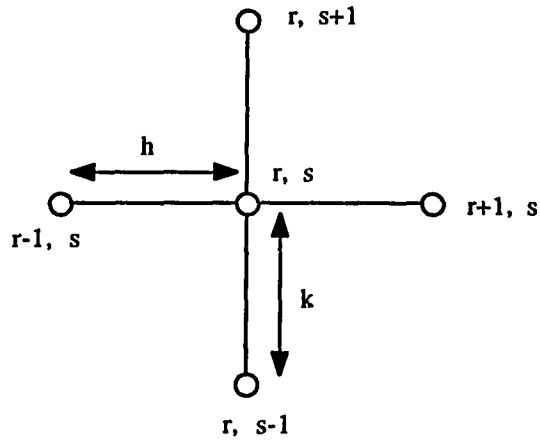

FIGURE 6: Points used in the finite difference method

where O(h) is the order of error. Also:

$$\frac{\partial u}{\delta y}_{r,s} \equiv u_y|_{r,s} \cong (U_{r,s+1} - U_{r,s}) / k + O(k)$$

Second-order accurate approximations to second order derivatives have the form:

$$\partial^2 u_{(r,s)} / \partial x^2 \equiv u_{xx}|_{r,s} \cong (U_{r+1,s} - 2U_{r,s} + U_{r-1,s}) / h^2 + O(h^2)$$

$$\partial^2 u_{(r,s)} / \partial y^2 \equiv u_{yy}|_{r,s} \cong (U_{r,s+1} - 2U_{r,s} + U_{r,s-1}) / k^2 + O(k^2)$$

Having developed an understanding of the finite difference approximation, let us now develop the representation we are concerned with. Consider the Laplace equation

$$\partial^2 u / \partial x^2 + \partial^2 u / \partial y^2 = 0$$

The procedure we adopt is the method of undetermined coefficients wherein we select, a priori, the points that we wish to use in the finite difference

approximation. They are shown in Figure 7. In this figure we have four different h_i and 4 nodal points. The point in the center is the one for which the difference equation is obtained.

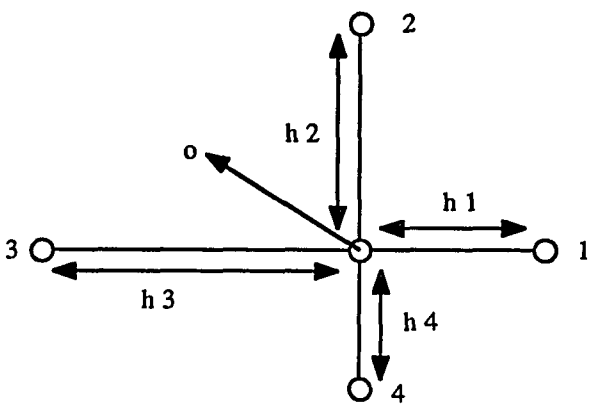

"o" : Grid point being computed.

FIGURE 7: Unequal spacing betwen points

The Laplace equation is represented as:

$$u_{xx} + u_{yy} = \sum_{i=0}^{4} \alpha_i U_i \qquad \text{-- (14)}$$

which can be interpreted as a weighted linear combination of the five selected points. The weights $\alpha_0,\ldots,\alpha_4$ are determined using Taylor series expansions. These are:

$$U_1 = U_0 + h_1 u_{x|0} + \frac{h_1^2}{2!} u_{xx|0} + \frac{h_1^3}{3!} u_{xxx|0} + \ldots,$$

$$U_2 = U_0 + h_2\, u_{y|0} + \frac{h_2^2}{2!} u_{yy|0} + \frac{h_2^3}{3!} u_{yyy|0} + \ldots,$$

$$U_3 = U_0 - h_3\, u_{x|0} + \frac{h_3^2}{2!} u_{xx|0} + \frac{h_3^3}{3!} u_{xxx|0} + \ldots,$$

here U_1, U_0, U_3 have the same y coordinate and U_2, U_0, U_4 the same x coordinate. Substituting these into (14) we get:

$$[u_{xx} + u_{yx}]\, 0 = [\alpha_0 + \alpha_1 + \alpha_2 + \alpha_3 + \alpha_4]\, U_0 + [\alpha_1 h_1 - \alpha_3 h_3]\, u_{x|0}$$

$$+ [\alpha_2 h_2 - \alpha_4 h_4]\, u_{y|0} + 1/2\, [\alpha_1 h_1^2 + \alpha_3 h_3^2]\, u_{xx|0}$$

$$+ 1/2\, [\alpha_2 h_2^2 + \alpha_4 h_4^2]\, u_{yy|0} + \sum_{i=1}^{4} [0(\alpha_i\, h_i^3)].$$

For the left side to equal the right side to equal O(h3) it is necessary that

$$\alpha_0 + \alpha_1 + \alpha_2 + \alpha_3 + \alpha_4 = 0$$

$$\alpha_1\, h_1 - \alpha_3 h_3 = 0$$

$$\alpha_2 h_2 - \alpha_4 h_4 = 0$$

$$\alpha_1 h_1^2 - \alpha_3 h_3^2 = 2$$

$$\alpha_2\, h_2^2 + \alpha_4\, h_4^2 = 2$$

The solution of these five equations is

$$\alpha_0 = -2\, [(1 / h_1 h_3) + (1 / h_2 h_4)] \quad , \quad \alpha_1 = \frac{2}{h_3(h_1+h_3)} \ ,$$

$$\alpha_2 = \frac{2}{h_2(h_2+h_4)} \quad , \quad \alpha_3 = \frac{2}{h_3(h_1+h_3)} \quad , \quad \alpha_4 = \frac{2}{h_4(h_2+h_4)} \ .$$

However, in our case $h_2 = h_4 = k$ and $h_1 = h_3 = h$ (Figure 6). Therefore, replacing 'u' by 'J' (current density symbol), we get:

$$\alpha_0 J_0 + \alpha_1 J_1 + \alpha_2 J_2 + \alpha_3 J_3 + \alpha_4 J_4 = jw\,\mu\,\sigma J_0 \qquad \text{-- (15)}$$

where, $\alpha_0 = -2\,(1/h^2 + 1/k^2)$, $\alpha_1 = 2/h^2$

$\alpha_2 = 2/k^2$, $\alpha_3 = 2/h^2$, $\alpha_4 = 2/k^2$

letting, $h_1 = h_3 = h = \Delta x$ and $h_2 = h_4 = k = \Delta y$

and substituting the explicit expression for the weights in (15) we obtain:

$$J_0 = \frac{1}{2\,(\Delta y^2 + \Delta x^2)}\,(\Delta y^2\,(J_1 + J_3) + \Delta x^2\,(J_2 + J_4) - j\omega\,\mu\,\sigma\,\Delta x^2\,\Delta y^2 J_0) \qquad \text{-- (16)}$$

where J_0 is the current value at the point being computed and is a complex quantity as explained earlier. Equation (16) is the finite difference approximation of the diffusion equation and is used to obtain the current values at all grid points.

2.4 Interpolation:

Having developed the finite difference technique, we now have a way of computing the current density at each point on the grid. The usage of the diffusion equation brings the effect of frequency into the current values computed at each point on the plate. The procedure which will be used for the numerical solution of the diffusion equation may be summarized as follows:

Starting with the D.C. value at each point on the grid we let the current redistribute itself over the plate until it reaches steady state. This section details the method used to obtain the initial D.C. current values from the UALGRL output file. The UALGRL output file has the following format:

Suppose the output file has 50 lines:

1 nx ny

where nx: Number of x intervals along the x axis.

ny: Number of y intervals along the y axis.

2 First Potential Value.

47 Last Potential Value.

48 Total current entering/leaving a current source/sink.

49 dx dy.

where dx: dimension of each x interval.

dy: dimension of each y interval.

50 conductivity of the plate in (mho/m).

The potential values in the UALGRL output file are obtained for the nodal points in a rectangular finite element grid as shown in Figure 8 below:

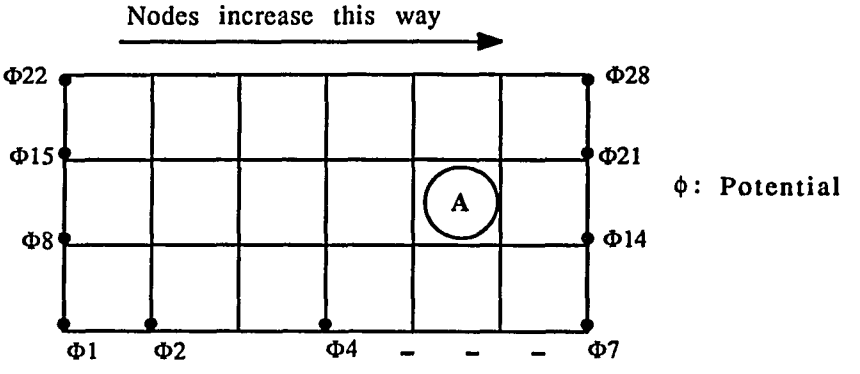

FIGURE 8: Format of UALGRL output file

The objective now is to utilize these values to get potential values at points within each rectangle "A". This is necessary because the grid used in computing the frequency dependent current is much finer than this grid. This is achieved by a straight forward interpolation technique.

Figure 9 depicts the finer grid resulting from the interpolation process. Only one rectangle is shown for simplicity.

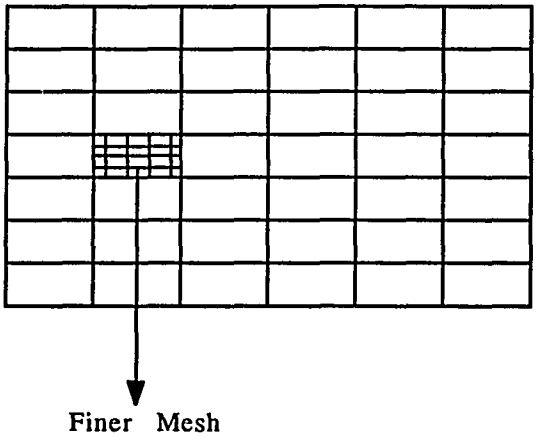

FIGURE 9 : Comparison of mesh size

The first step in interpolation is to understand the usage of the coordinate system. Interpolation functions for rectangular elements with sides parallel to the global axis are easily developed using Lagrangian interpolation concepts. Figure 10 below, shows the rectangle with its global coordinates. For the 4-node rectangle in our case, the functions in terms of the local coordinates are:

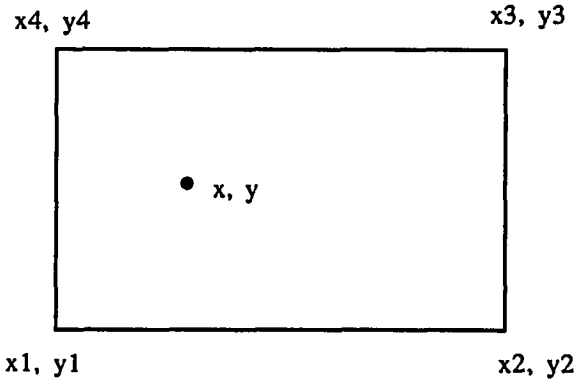

FIGURE 10 : Interpolation axis

$$\phi(v,w) = \phi_1 N_1(v,w) + \phi_2 N_2(v,w) + \phi_3 N_3(v,w) + \phi_4 N_4(v,w)$$

where ϕ is the potential.

where $N_1(v,w) = L_1(v)L_1(w)$

$N_2(v,w) = L_2(v)L_2(w)$

$N_3(v,w) = L_3(v)L_3(w)$

$N_4(v,w) = L_4(v)L_4(w)$

and the L_i are the lagrange polynomials. The L_i function is a product of n linear factors. Interpolation functions formed as products in this way satisfy the requirements of possessing unit value at the node for which they are defined and zero value at the other nodes.

The interpolation function in this case is:

$$N_i(v,w) = \frac{1}{4}(1 + vv_i)(1 + ww_i) \qquad -- \quad (17)$$

where -1<= v <=1 and -1<= w <=1, and i = 1, 2, 3, and 4 for the four nodes of the rectangle. The v and w axis are the coordinate axis for the local coordinate system.We now need to develop a mapping technique to make the (v,w) coordinate system correspond to the (x,y) coordinate system that we use. In order to do this let us look at Figure 11.

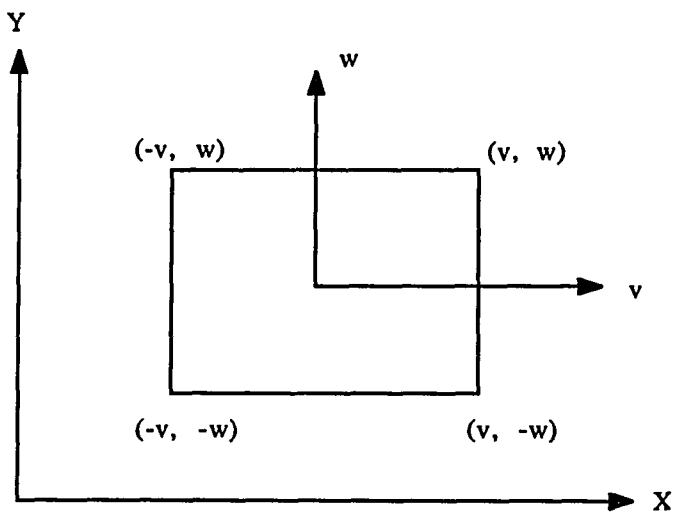

FIGURE 11: Coordinate system

Given the previous information, we need to develop relations between x and v and y and w.

Now, $x_1 = x_4 = x_a$ $\qquad$ $x_1 = y_2 = y_a$

also

$x_2 = x_3 = x_b$ $\qquad$ $y_3 = y_4 = y_b$

Therefore from (17), after substituting the v and w values for the four nodes of our rectangle and utilising the two identities

$$x = \sum_{i=1}^{4} N_i(v, w)x_i \text{ and } y = \sum_{i=1}^{4} N_i(v, w)y_i \text{ we get,}$$

$$4x = x_a (1 - v)(1 - w) + x_b(1 + v)(1-w) + x_b(1 + v)(1 - w) + x_a(1 - v)(1 + w)$$

or

$$4x = 2x_a(1 - v) + 2x_b(1 + v)$$

or

$$2x = (x_a + x_b) + (x_b - x_a)v$$

or

$$v = 2x / (x_b - x_a) - (x_b + x_a) / (x_b - x_a)$$

Therefore, $\partial v / \partial x = 2 / (x_b - x_a)$, $\partial v / \partial y = 0$

For a mapping relation between w and y we have similarly:

$$4y = y_a(1 - v)(1 - w) + y_a(1 + v)(1 - w) + y_b(1 + v)(1 + w) + y_b(1 - v)(1 + w)$$

or

$$4y = 2y_a(1 - w) + 2y_b(1 + w)$$

or

$$2y = y_a + y_b + w(y_b - y_a)$$

or

$$w = 2y / (y_b - y_a) - (y_a + y_b) / (y_b - y_a)$$

Therefore, $\partial w / \partial y = 2 / (y_b - y_a)$, $\partial w / \partial x = 0$

Now we know that, $\phi = \sum_{i=1}^{4} \phi_i N_i$

and $$\frac{\partial \phi}{\partial x} = \sum_{i=1}^{4} \phi_i \frac{\partial N_i}{\partial x}$$

where $$\frac{\partial N_i}{\partial x} = \frac{\partial N_i}{\partial v}\frac{\partial v}{\partial x} + \frac{\partial N_i}{\partial w}\frac{\partial w}{\partial x}$$

But $\frac{\partial w}{\partial x} = 0$, Therefore we have,

$$\frac{\partial N_i}{\partial x} = \frac{\partial N_i}{\partial v}\frac{\partial v}{\partial x}$$

Similarly $\frac{\partial N_i}{\partial y} = \frac{\partial N_i}{\partial w}\frac{\partial w}{\partial y}$ where $\frac{\partial v}{\partial y} = 0$

Therefore: $\frac{\partial \phi}{\partial x}$ at any point on the plate is given by:

$$\frac{\partial \phi}{\partial x} = \phi 1 \frac{\partial N1}{\partial x} + \phi 2 \frac{\partial N2}{\partial x} + \phi 3 \frac{\partial N3}{\partial x} + \phi 4 \frac{\partial N4}{\partial x}$$

$$= \phi 1 \frac{\partial N1}{\partial v}\frac{\partial v}{\partial x} + \phi 2 \frac{\partial N2}{\partial v}\frac{\partial v}{\partial x} + \phi 3 \frac{\partial N3}{\partial v}\frac{\partial v}{\partial x} + \phi 4 \frac{\partial N4}{\partial v}\frac{\partial v}{\partial x}$$

From (17) we have $\frac{\partial N1}{\partial w} = \frac{1}{4}(1 + vv1)\, w1$

Similarly for points 2, 3, and 4

Substituting in the equation we get:

$$\partial\phi / \partial x =$$

$$\phi 1/4 \left[1 + \left(\frac{2y}{y4-y1} - \frac{y4+y1}{y4-y1} \right) \left(\frac{2y1}{y4-y1} - \frac{y4+y1}{y4-y1} \right) \left(\frac{4x1}{(x3-x4)^2} - \frac{2(x3+x4)}{(x3-x4)^2} \right) \right]$$

$$+$$

$$\phi 2/4 \left[1 + \left(\frac{2y}{y4-y1} - \frac{y4+y1}{y4-y1} \right) \left(\frac{2y2}{y4-y1} - \frac{y4+y1}{y4-y1} \right) \left(\frac{4x2}{(x3-x4)^2} - \frac{2(x3+x4)}{(x3-x4)^2} \right) \right]$$

$$+$$

$$\phi 3/4\left[1+\left(\frac{2y}{y4-y1}-\frac{y4+y1}{y4-y1}\right)\left(\frac{2y3}{y4-y1}-\frac{y4+y1}{y4-y1}\right)\left(\frac{4x3}{(x3-x4)^2}-\frac{2(x3+x4)}{(x3-x4)^2}\right)\right]$$

$$+$$

$$\phi 4/4\left[1+\left(\frac{2y}{y4-y1}-\frac{y4+y1}{y4-y1}\right)\left(\frac{2y4}{y4-y1}-\frac{y4+y1}{y4-y1}\right)\left(\frac{4x4}{(x3-x4)^2}-\frac{2(x3+x4)}{(x3-x4)^2}\right)\right]$$

Similarly for $\frac{\partial\phi}{\partial y}$ we have:

$$\frac{\partial\phi}{\partial y}=\phi 1\frac{\partial N1}{\partial y}+\phi 2\frac{\partial N2}{\partial y}+\phi 3\frac{\partial N3}{\partial y}+\phi 4\frac{\partial N4}{\partial y}$$

$$=\phi 1\frac{\partial N1}{\partial w}\frac{\partial w}{\partial y}+\phi 2\frac{\partial N2}{\partial w}\frac{\partial w}{\partial y}+\phi 3\frac{\partial N3}{\partial w}\frac{\partial w}{\partial y}+\phi 4\frac{\partial N4}{\partial w}\frac{\partial w}{\partial y}$$

From (17) we have: $\frac{\partial N1}{\partial w}=\frac{1}{4}(1+vv1)w1$

and similarly for points 2, 3 and 4, substituting in the equation we get:

$\partial\phi/\partial y =$

$$\phi 1/4\left[1+\left(\frac{2x}{x3-x4}-\frac{x3+x4}{x3-x4}\right)\left(\frac{2x1}{x3-x4}-\frac{x3+x4}{x3-x4}\right)\left(\frac{4y1}{(y4-y1)^2}-\frac{2(y1+y4)}{(y4-y1)^2}\right)\right]$$

$$+$$

$$\phi 2/4\left[1+\left(\frac{2x}{x3-x4}-\frac{x3+x4}{x3-x4}\right)\left(\frac{2x2}{x3-x4}-\frac{x3+x4}{x3-x4}\right)\left(\frac{4y2}{(y4-y1)^2}-\frac{2(y1+y4)}{(y4-y1)^2}\right)\right]$$

$$+$$

$$\phi 3/4\left[1+\left(\frac{2x}{x3-x4}-\frac{x3+x4}{x3-x4}\right)\left(\frac{2x3}{x3-x4}-\frac{x3+x4}{x3-x4}\right)\left(\frac{4y3}{(y4-y1)^2}-\frac{2(y1+y4)}{(y4-y1)^2}\right)\right]$$

$$+$$

$$\phi 4/4\left[1+\left(\frac{2x}{x3-x4}-\frac{x3+x4}{x3-x4}\right)\left(\frac{2x4}{x3-x4}-\frac{x3+x4}{x3-x4}\right)\left(\frac{4y4}{(y4-y1)^2}-\frac{2(y1+y4)}{(y4-y1)^2}\right)\right]$$

We thus have a way to compute $\frac{\partial \phi}{\partial x}$ and $\frac{\partial \phi}{\partial y}$.

Certain important conditions need to be kept in mind while we compute the derivatives. These are explained with reference to Figure 12 and 13.

For $\frac{\partial \phi}{\partial x}$: while computing $\frac{\partial \phi}{\partial x}$ at node points like x, which lie on the boundaries of elements of the grid(from Figure 12), the value is obtained by averaging 'x-1' and 'x+1'. There is no x component of current along side 1 and side 2.

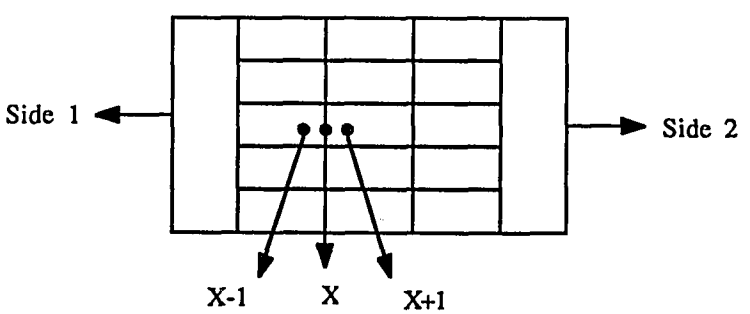

FIGURE 12: Averaging for initial Jx

For $\frac{\partial \phi}{\partial y}$: While computing $\frac{\partial \phi}{\partial y}$ at node points like y which lie along the boundaries of the elements of the grid(from Figure 13) the value is obtained by averaging 'y-1' and 'y+1'. There is no y component of current along side 3 and side 4.

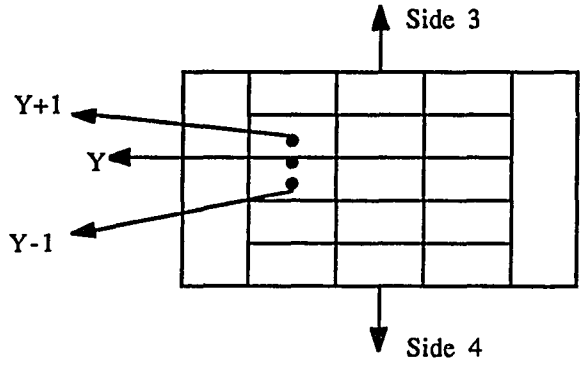

FIGURE 13 : Averaging for initial Jy

Thus we have developed the method to compute $\frac{\partial\phi}{\partial x}$ and $\frac{\partial\phi}{\partial y}$ at each grid point on the finer grid. Once this is done, the next step is to compute J_x and J_y at each point on this grid. These then serve as "initial conditions" for the frequency dependent current equation. More specifically, from ohm's law

$$\bar{J} = -\sigma\nabla\phi ,$$

J_x is obtained at each point by:

$$J_x = -\sigma \frac{\partial\phi}{\partial x}$$

and J_y is obtained at each point by:

$$J_y = -\sigma \frac{\partial\phi}{\partial y} .$$

2.5 Iterative and Boundary Conditions:

In the previous sections we developed the theory needed to compute the DC current distribution on the plane. Our approach is then to solve the Helmholtz equation, obtained from the diffusion equation under time-harmonic conditions, in an iterative way to obtain the frequency dependent current distribution.

After experimenting with several iterative techniques, we finally decided to use the so called simultaneous over-relaxation method [1] with a slight modification. This technique had to be modified because the current values do not converge with the original technique. Moreover, it was found that the iteration technique had to be developed carefully as the current values are sensitive to the way the iteration is done. More specifically, the following methodology was found to be optimum:

a) We start the iteration from the center most row of the grid and proceed towards the top and bottom boundaries one at a time. The row above the middle most row is iterated before the row lying immediately below the center row.

b) Within each row the point in the middle is iterated first and we then proceed towards the left and right boundaries, iterating each point alternatively. This is shown in Figure 14.

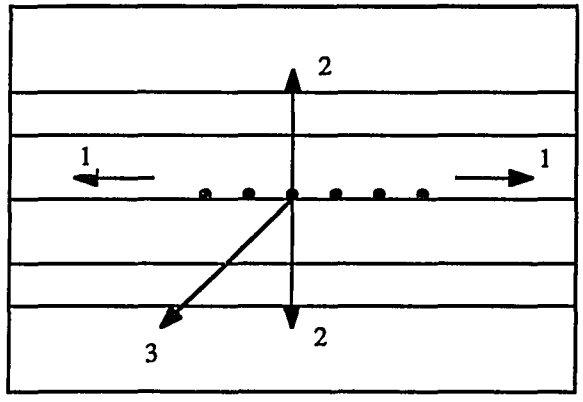

3: Center most point of the row in the center of the grid.

1: First iterate towards left and right from the center point.

2: Then move towards the upper and lower rows in the grid.

FIGURE 14 : Illustration of iterative technique

A point on the grid is said to have converged if the below mentioned condition is met:

Let U_0 be the current value at any point on the grid. As we iterate each point on the grid several times, we have 2 sets of values for each point, namely: $U_{(new)}$ and $U_{(old)}$

We can therefore say that a point is converged if:

$$|U_{(new)} - U_{(old)}| / |U_{(old)}| \leq \text{"convergence tolerance"}$$

where "convergence tolerance" is a number specified in the input file of the program and can vary depending upon the desired level of accuracy. Generally speaking, a convergence tolerance of ".001" is sufficient for most cases. As already mentioned, in order to obtain faster convergence, we utilize

a slightly modified version of SOR or "Simultaneous Over Relaxation," and the parameter associated with it is 'a' the overrelaxation parameter. This lies between: $1< a <2$.

In this scheme, the previous current value at the point being computed is utilized to obtain the present current value. Thus, equation (16) with this method will become:

$$J_0 = \frac{1}{2(\Delta y^2 + \Delta x^2)} (\Delta y^2 (J_1 + J_3) + \Delta x^2 (J_2 + J_4) - j\omega \mu \sigma \Delta x^2 \Delta y^2 J_{0(previous)}) \quad \text{-- (18)}$$

From equation (18) we know how to compute J_0 at each grid point. Let us see how the parameter 'a' helps in faster convergence. Basically, every time we compute 'J_0' at a grid point, we obtain a new weighted average for J_0 by utilizing this parameter. In equation form:

Let J_0 be J^*, therefore J_{new} is obtained by:

$$J_{new} = aJ^* + (1 - a) J_{previous}$$

When we start the first iteration, "$J_{previous}$" at every point is taken to be the value at the DC current density. Thus, we compute J^* for a point, then J_{new} and utilize this J_{new} to compute J^* for the next point. There is no fixed way to

determine the correct value for 'a.' This is a weakness of the SOR technique. The best way is to start with a higher value and move to a lower value to obtain

faster convergence. The boundary conditions on the plane for the iterative process are as follows:

-- The points on the plane and hole (if it exists) boundary are not iterated. These points get their value from the points immediately preceding them in the grid and an exponential factor based on the discretization distance and skin depth.

Equation (18) changes for certain points while computing the 'J_x' ('x' current component at all grid points) and 'J_y' ('y' current component at all grid points). Since in either case the grid points on the boundary are not computed, the change in equation (18) is limited to points lying next to the edges for both J_y and J_x. Let us now see how the equation changes in both the cases.

For Jx: Consider figure 15. It shows the points for which the equation changes. For the points above the lower edge:

$$J_0 = \frac{1}{(2(\Delta y^2 + \Delta x^2) - \Delta x^2 e^{\Delta y/\delta})} \left(\Delta y^2 (J_1 + J_3) + \Delta x^2 J_2 - j\omega \mu \sigma \Delta x^2 \Delta y^2 J_0(\text{prev.}) \right)$$

where δ: skin depth

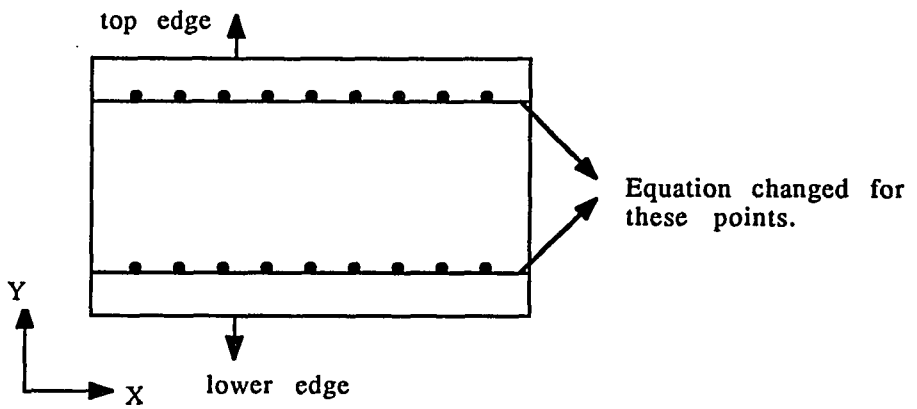

FIGURE 15 : Boundary points for which Jx equation changes

Similarly, for the points below the top edge:

$$J_0 = \frac{1}{(2(\Delta y^2 + \Delta x^2) - \Delta x^2 e^{\Delta y/\delta})} (\Delta y^2(J1 + J3) + \Delta x^2 J_4 - j\omega\mu\sigma\Delta x^2\Delta y^2 J_0(\text{prev.}))$$

The numbering of the points is shown in Figure 6.

For J_y: Consider figure 16. For the points next to the left edge, the equation becomes

$$J_0 = \frac{1}{(2(\Delta y^2 + \Delta x^2) - \Delta\, y^2\, e^{\Delta y/\delta})} (\Delta y^2 J_1 + \Delta x^2(J2 + J4) - j\omega\,\mu\,\sigma\,\Delta\, x^2\,\Delta\, y^2 J_0(\text{prev.}))$$

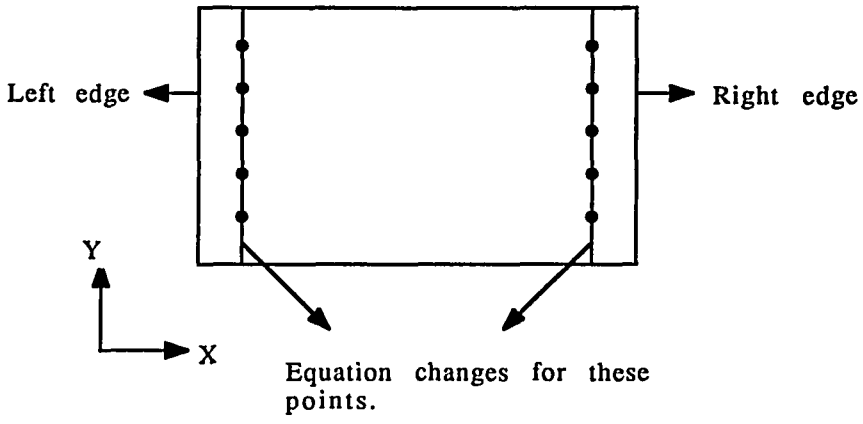

FIGURE 16 : Boundary points for which Jy equation changes

Similarly for points next to the right edge the equation becomes:

$$J_0 = \frac{1}{(2(\Delta y^2 + \Delta x^2) - \Delta y^2 e^{\Delta y/\delta})} \quad (\Delta y^2 J_3 + \Delta x^2(J_2 + J_4) - j\omega\mu\sigma\Delta x^2\Delta y^2 J_0(\text{prev.}))$$

The final value of the current at each point is obtained after a series of iterations till the point converges. Some boundary points are illustrated in Figure 17 for a plane with a perforation.

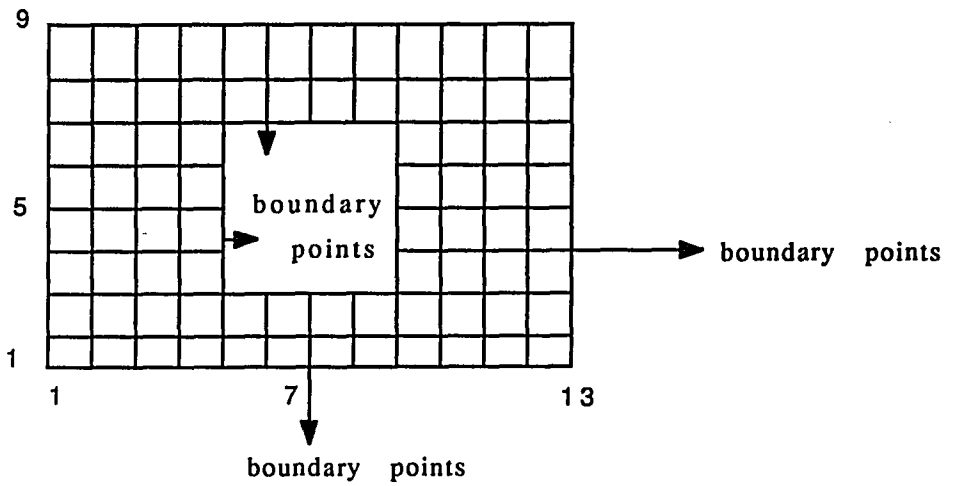

Figure 17: Points not iterated upon

Let us now see how we arrive at the exponential factor required for this multiplication. Consider Figure 18:

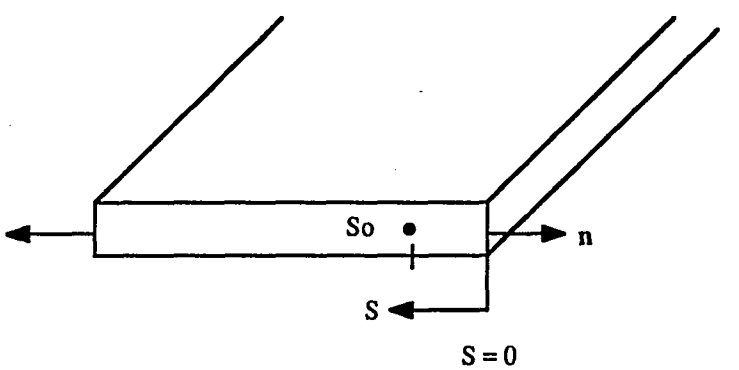

FIGURE 18: Model for exponential factor

Let J(o) be the value of the current density tangential to the edge of the plane. We know that: $J(s) = J(o)e^{-s/\delta}$

where δ: skin depth = $\left(\frac{1}{\pi f \mu \sigma}\right)^{1/2}$

Thus for a point at s = so we have,

$$J(so) = J(o)e^{-so/\delta}$$

from which,

$$J(o) = J(so)e^{so/\delta}$$

Using so = Δx or Δy depending on which side the point is located, the boundary values can be obtained from the values at the adjacent interior nodes. While computing J_x or the 'x' component of current density on the grid, the boundary conditions can be represented as:

$$J(c) = J(b)\, e^{\Delta y/\delta}$$

and for the hole: $J(d) = J(a)\, e^{\Delta y/\delta}$ where points a, b, c, d are shown in Figure 19.

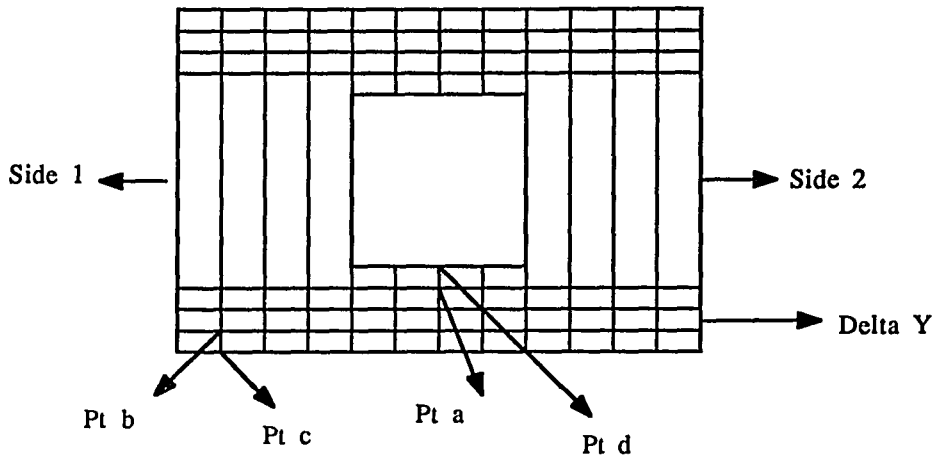

(Note that the grid is shown this way for explanation only and the same condition applies to the upper boundary)

FIGURE 19: Representation of boundary points for Jx

Similarly, while computing Jy or the 'y' component of current density on the grid, the boundary conditions can be represented as:

$$J(c) = J(b)e^{\Delta x/\delta}$$

and for the hole: $J(d) = J(a)e^{\Delta x/\delta}$ where points a, b, c, d are shown in Figure 20.

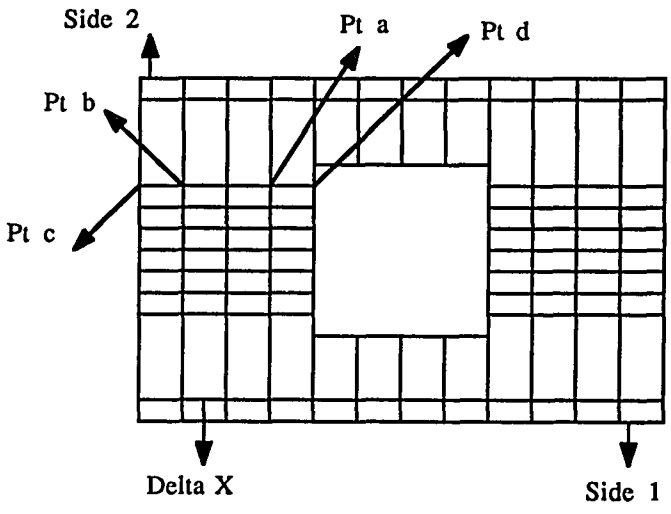

(Note that the grid is shown this way for explanation only and the same condition applies to the right boundary)

FIGURE 20: Representation of boundary points for Jy

2.6 Resistance and Inductance Calculation

In the previous sections we developed the finite difference technique to solve the diffusion equation under time harmonic conditions for the frequency dependent current densities on a ground plane. In this section we show how to compute the resistance (R) and inductance (L) of the ground plane given the DC and frequency dependent current distribution.

Resistance computation:

Let 'v' be the volume the conducting plane occupies. Inside v, the electric field is given by:

$$\bar{E} = -\nabla\phi - j\omega\ \bar{A}$$

where ϕ denotes the electric potential and w is the radian frequency. The frequency dependent current density in v is given by:

$$\bar{J}_{ac} = -\sigma\nabla\phi - j\omega\sigma\ \bar{A} \qquad \text{-- (19)}$$

The time average power dissipation in a steady state situation is given by:

$$W_j = \frac{1}{\sigma}\int_v \left(\bar{J}^*_{ac} \cdot \bar{J}_{ac} \right) dv$$

which under the assumption of uniform current distribution within the thickness of the plane t becomes,

$$W_j = \frac{1}{\sigma}(t)\int_s \left(\bar{J}^*_{ac} \cdot \bar{J}_{ac} \right) dv \qquad \text{-- (20)}$$

The term inside the integral in equation (19) can be written as:

$$(\bar{J}^*_{ac} \cdot \bar{J}_{ac}) = |\bar{J}_{ac}|^2 = (|J_x|^2 + |J_y|^2)$$

Let,

$$J_r(\text{all over the plane}) = (|J_x|^2 + |J_y|^2)$$

Thus we need to compute J_r over the entire conducting plane. Since our plane is broken up into several elements we can compute J_r for each element and then add all of them to calculate W_j . Each element for which this is done corresponds to the one obtained from UALGRL. To compute J_r for each grid we utilize an interpolation scheme similar to that described in section(2.4) which gives us J_r at any point within one element of the plane, knowing the J_r's at the four corners of the element. This is shown below in figure (21).

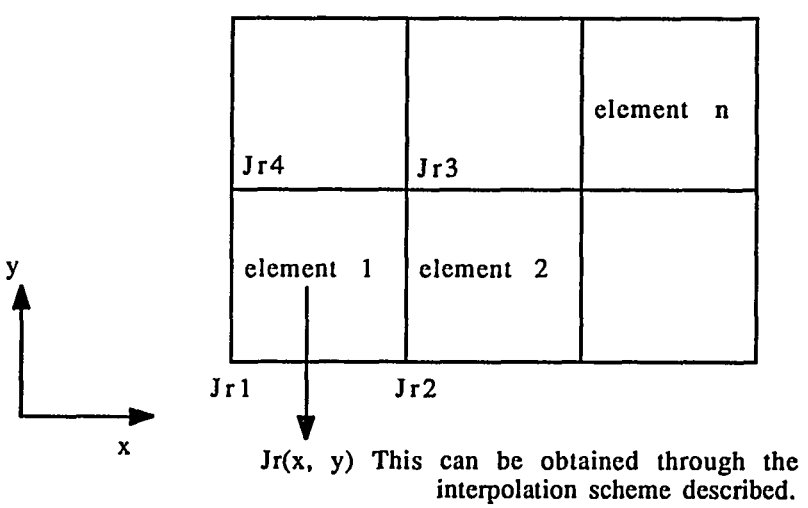

FIGURE 21: Interpolation scheme used for resistance computation

From figure (21) we see that if we know the J_r's at the four corners of every element we can obtain J_r as a function of x and y inside the element. Let us now compute $J_r(x, y)$ for one element. Figure (22) below shows the element being utilized:

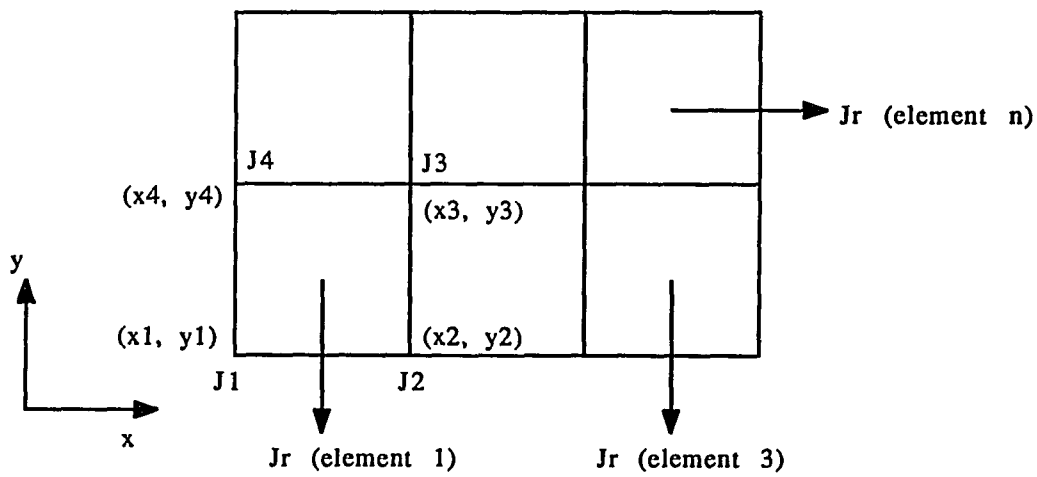

FIGURE 22: Actual grid used to perform integration in resistance computation

We will denote the total current contributions due to all elements in the plane as J (from all elements), obtained after the surface integral in equation (20). Therefore, we have:

$$W_j = J \text{ (from all elements)} * t / \sigma = R|I_{tot}|^2$$

where R: is the resistance of the plane

and I_{tot}: the total current flowing out of the sources into the sinks.

or

$$J_{r(\text{element } 1)} + J_{r(\text{element } 2)} + \text{- - - - - - +} J_{r(\text{element } n)} = (\sigma)\ (R|I_{tot}|^2) / t$$

'R' can now be easily determined as:

$$R = t\ [J_{r(\text{element } 1)} + J_{r(\text{element } 2)} + \text{- - - - - - +} J_{r(\text{grid } n)}] / (\sigma)\ (|I_{tot}|^2)$$

The surface integral from equation (20) can be represented as:

$$\int_s\ [J_{r(\text{element } 1)} + J_{r(\text{element } 2)} + J_{r(\text{element } 3)} + \text{- - - -} + J_{r(\text{grid } n)}]\ dS$$

or, for 'element 1' we have,

$$\int_s\ [J_{r(\text{element } 1)}\ dS$$

which can be written as:

$$\int_s\ [J_{r(\text{element } 1)}\ dS = \int_s J_1 N_1 dS + \int_s J_2 N_2 dS + \int_s J_3 N_3 dS + \int_s J_4 N_4 dS \quad \text{—(21)}$$

If we solve one of these integrals, the result for the other three can be obtained from it's result with a slight change. The procedure to solve the integrals for the other grids is exactly the same as that for the first one.

Now $\int_S J_1 N_1 dS = \int_S J_1/4\,[\,(1 + vv_1)(1 + ww_1)\,]\,dS$ — from eqn (17)

This interpolation is exactly the same as that done for potential values from UALGRL in order to get the initial DC current distributions, except that now we are using current at the four corners of each element instead of potential.Substituting the values of 'v' and 'w' in terms of 'x' and 'y' as derived in section 2.4, we get:

$$\int_S J_1 N_1 dS = \int_S J_1/4[1 + \left(\frac{2x}{x3-x4} - \frac{x3+x4}{x3-x4}\right)\left(\frac{2x1}{x3-x4} - \frac{x3+x4}{x3-x4}\right) *$$

$$[1 + \left(\frac{2y}{y4-y1} - \frac{y4+y1}{y4-y1}\right)\left(\frac{2y1}{y4-y1} - \frac{y4+y1}{y4-y1}\right)]\,dS \quad — (22)$$

Now $\left(\frac{2x1}{x3-x4} - \frac{x3+x4}{x3-x4}\right)$ is a constant . Let us call it C_1.

Also $\left(\frac{2y1}{y4-y1} - \frac{y4+y1}{y4-y1}\right)$ is a constant. Let us call it C_2.

Therefore eqn (22) becomes:

$$\int_S J_1 N_1 dS = \int_S J_1/4[1 + (C_1 \frac{2x}{x3-x4} - C_1 \frac{x3+x4}{x3-x4})] *$$

$$[1 + (C_2 \frac{2y}{y4-y1} - C_2 \frac{y4+y1}{y4-y1})]\,dS$$

Now $C_1 \frac{2}{x_3-x_4}$ is a constant. Let us call it C_3 .

Also $C_1\left(\frac{x_3+x_4}{x_3-x_4}\right)$ is a constant. Let us call it C_4

Similarly $C_2 \frac{2}{y_4-y_1}$ is called C_5 and $C_2\left(\frac{y_4+y_1}{y_4-y_1}\right)$ is called C_6.

So eqn (22) becomes,

$$\int_s J_1 N_1 \, dS = \int_s J_1/4 \, [1 + (C_3x - C_4)] * [1 + (C_5y - C_6)] \, dS$$

Integrating with respect to 'x' first and then 'y' and substituting the limits we get the following result:

$$\int_s J_1 N_1 \, dS = J_1/4 \, [(x_3-x_4)(y_4-y_1) + C_5 (x_3-x_4)(y_4^2/2 - y_1^2/2) - C_6 (x_3-x_4)(y_4-y_1) +$$

$$C_3 (x_3^2/2 - x_4^2/2)(y_4-y_1) + C_3 C_5 (x_3^2/2 - x_4^2/2)(y_4^2/2 - y_1^2/2) -$$

$$C_3 C_6 (x_3^2/2 - x_4^2/2)(y_4-y_1) - C_4 (x_3-x_4)(y_4-y_1) - C_4 C_5 (x_3-x_4)(y_4^2/2 - y_1^2/2) +$$

$$C_6 C_4 (x_3-x_4)(y_4-y_1)] \qquad \text{— eqn (23)}$$

Looking at equation (23) we can see why integrating equation (21) is merely repeating equation (23) with the constants C_1 and C_2 changing their respective 'x' and 'y' coordinates depending on the node involved in the

integration. Thus equation (21) is merely an addition of four equations similar to equation (23) but with different constant values. This can be written as:

$$\int_s [J_{r(\text{grid } 1)}\, dS = J_1/4\ [\text{eqn (22)}] + J_2/4\ [---] + J_3/4\ [---] + J_4/4\ [---] \quad \text{-- eqn (24)}$$

where the brackets are basically eqn (23) modified with C_1 and C_2 taking different values. Thus the total current density in element 1 is obtained through an interpolation scheme. A closer look at equation (24) reveals, that integrating for current in the other elements, namely element 2, element 3 etc can be performed in exactly the same way with the basic format of equation (23) and equation (24) remaining intact. The only change would be in the coordinates involved depending on the element being integrated upon and the total current is then obtained by adding up the contributions due to each element.

Inductance Computation:

The inductance of a ground plane is computed in exactly the same manner as described for the resistance with the basic formula being:

$$W_m = \int_v (\bar{J}^*_{ac} \cdot \bar{A}) dv = L|I_{tot}|^2$$

where L: is the inductance of the plane

W_m: the time average magnetic energy in a steady state situation.

and $\bar{A}$ is obtained as $-j\omega\sigma \bar{A} = \bar{J}_{ac} - \bar{J}_{dc}$ (from eqn 19)

The term $\bar{J}_{dc}$ is an approximation of ($-\sigma \nabla\phi$), where 'ϕ' is the electric potential.This approximation was used in calculating the magnetic vector potential in this methodology.

However, it was found that calculating 'A' numerically by equation (19) does not provide the necessary accuracy required for obtaining accurate values of L. An alternative approach which has not been considered here is to obtain $\bar{A}$ directly by integrating over the current distribution in the plane. This approach should be accurate provided the calculated current distribution is accurate. The accuracy of the current distribution is examined in the following chapter. Further work needs to be done in this area

CHAPTER 3

3.1 Observations

The following observations can be made regarding the frequency dependent current distribution over a lossy ground plane obtained numerically using the aforementioned procedure and the methodology described in the preceeding chapters to compute the plane parasitics.

The observations are based on surface plots for the current distribution for specific plane geometries. The plane geometries used to test the program are shown in Figure 23 and then in Figure 38. The surface plots correspond to frequencies of 5, 10 and 25 MHz. Surface plots for frequencies higher than these could not be plotted due to memory constraints since the fineness of the numerical grid resulted in very large arrays at these frequencies. The specific values of 'dx' and 'dy' and the size of the grids is shown below:

Frequency	Size of grid	dx	dy
5 MHz	120 by 120	0.25 mm	0.25 mm
10 MHz	240 by 240	0.125 mm	0.125 mm
25 MHz	480 by 480	0.0625 mm	0.0625 mm

The choice of dx and dy is governed by the skin depth at the frequency of operation and is related to the skin depth. For lower frequencies it is "skin depth / 4" and as we go to higher frequencies it becomes "skin depth / 8". In

order to get a physical picture of the current distribution in the plane and accomodate the limitations of the plotting software, the arrays sizes were reduced. The number of points being represented for the chosen frequencies are:

Frequency	Points along 'x'	Points along 'y'	Actual grid
5 MHz	60	120	120 by 120
10 MHz	60	120	240 by 240
25 MHz	60	120	480 by 480

Since the y current component has even symmetry and the x current component odd symmetry for the problem considered, the entire plot can be visualized by looking at half the plane for either case. The chosen plane configuration has the source and sink point located at the plane center along the x axis and directly opposite each other, which makes it easier to analyse the plots. The behavior of the current with increasing frequency leads us to the following conclusions:

1) The current distribution at DC is fairly uniform over the plane except in the vicinity of the source/sink where it assumes its peak value. This is true for both the 'x' and 'y' current components.

2) With increasing frequency the current redistributes itself throughtout the plane, though without much change at least for the frequencies considered. This is illustrated in the surface plots shown for a plane without perforation. For a plane with perforation, the current crowds around the edges of the hole

and this crowding increases as frequency increases. The 'y' current component is strong along the vertical edges of the perforation and the 'x' component along the horizontal as expected. This supports the fact of current trying to flow along narrow paths with increase in frequency. Figure 23 shows the plane geometry used for the first series of plots. It can be seen in the plots that as the frequency increases, the concentration of the peaks seen around the source and sink increases as expected from the fact that the skin depth and thus the extent of diffusion decreases. This results in sharper peaks around the source/sink points.

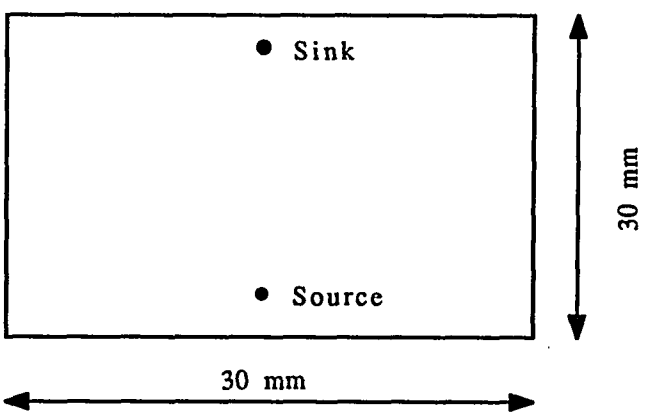

THICKNESS: 1.0 mm
CONDUCTIVITY: 58.0 mho/mm
PERMEABILITY: 12.56E-10 H/mm

SOURCE LOCATION: X = 15, Y = 5
SINK LOCATION: X = 15, Y = 25

FIGURE 23: Plane without perforation

SURFACE PLOTS OF PLANE CURRENT DENSITY

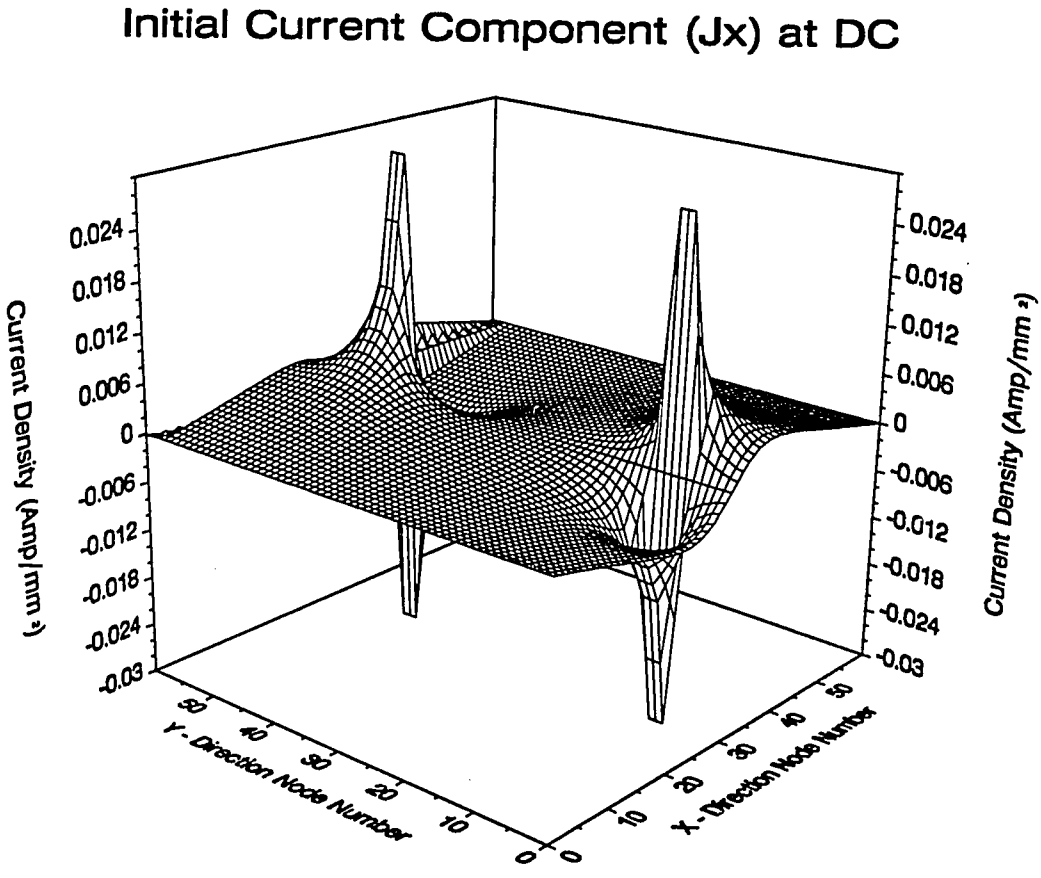

FIGURE 24: Initial current component (Jx) at DC

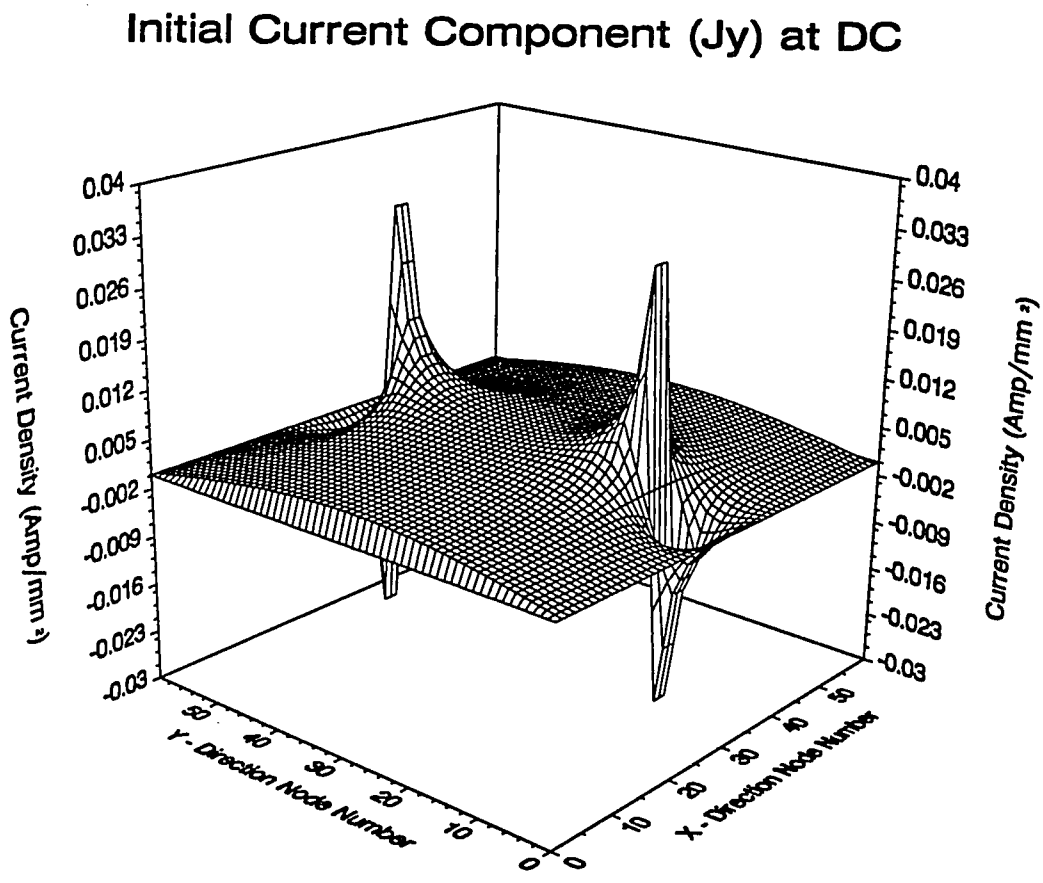

FIGURE 25: Initial current component (Jy) at DC

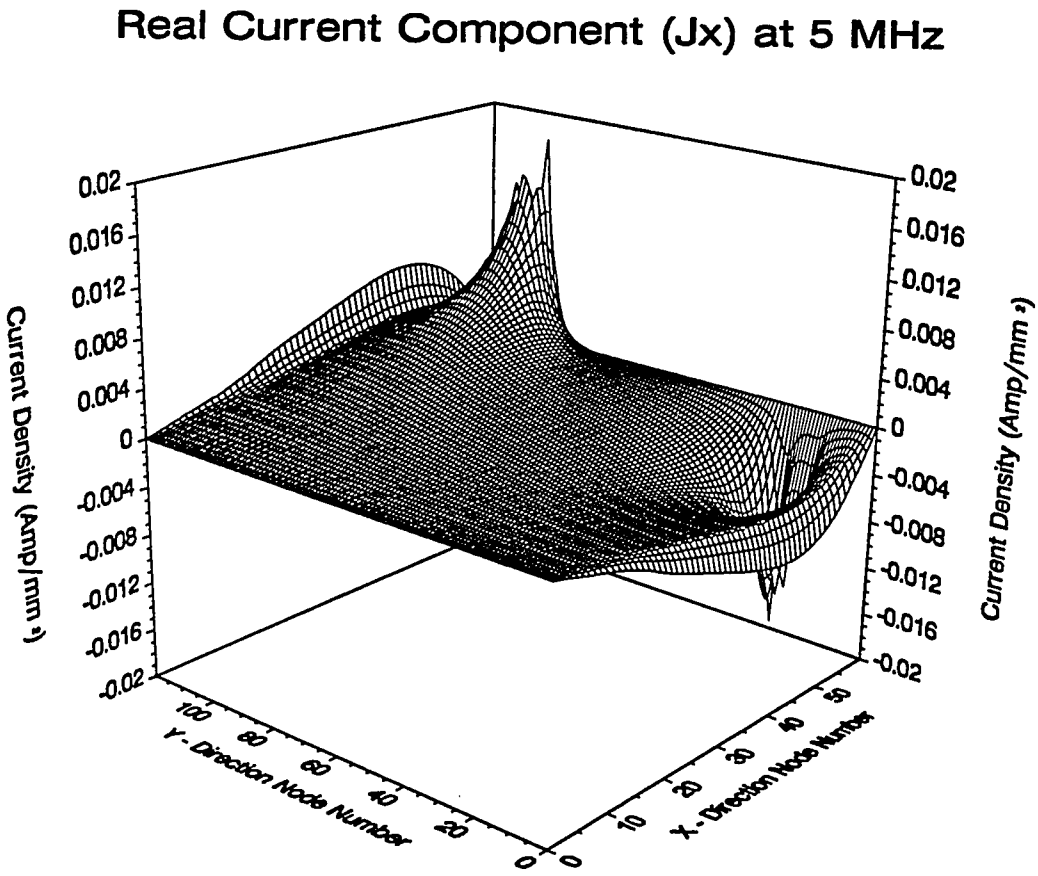

FIGURE 26: Real current component (Jx) at 5 MHz

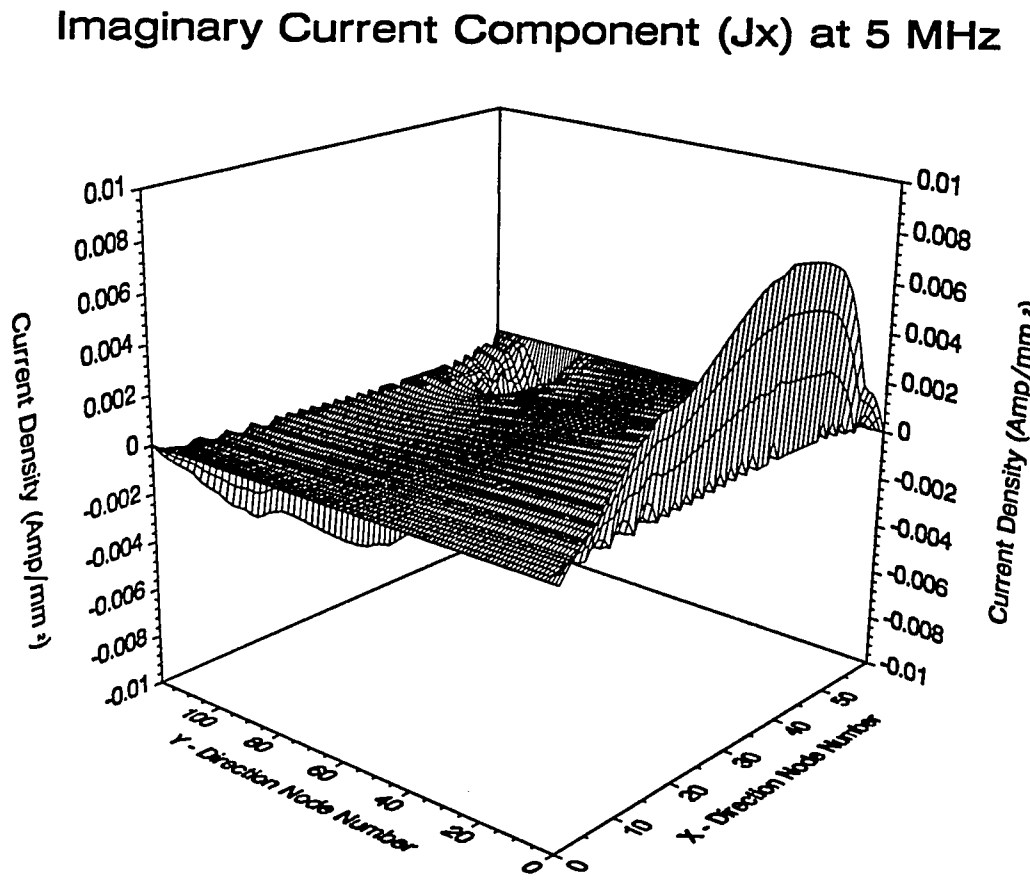

FIGURE 27: Imaginary current component (Jx) at 5MHz

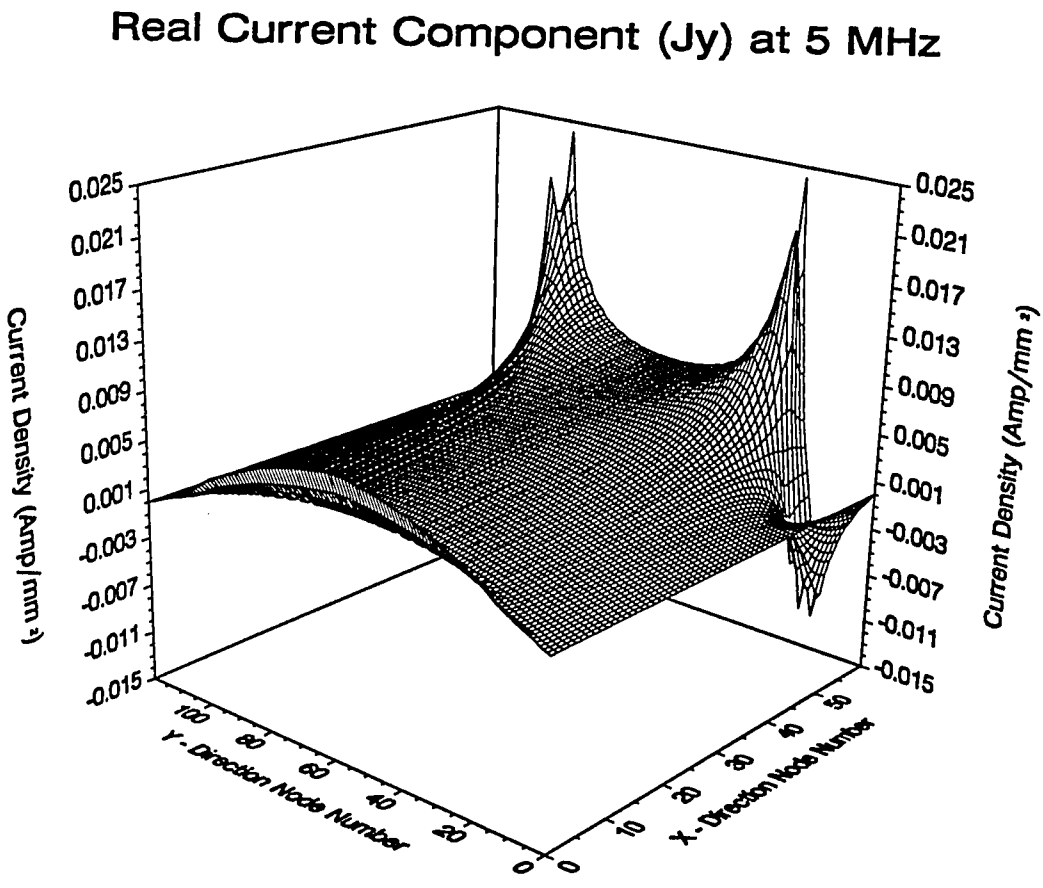

Figure 28: Real current component (Jy) at 5 MHz

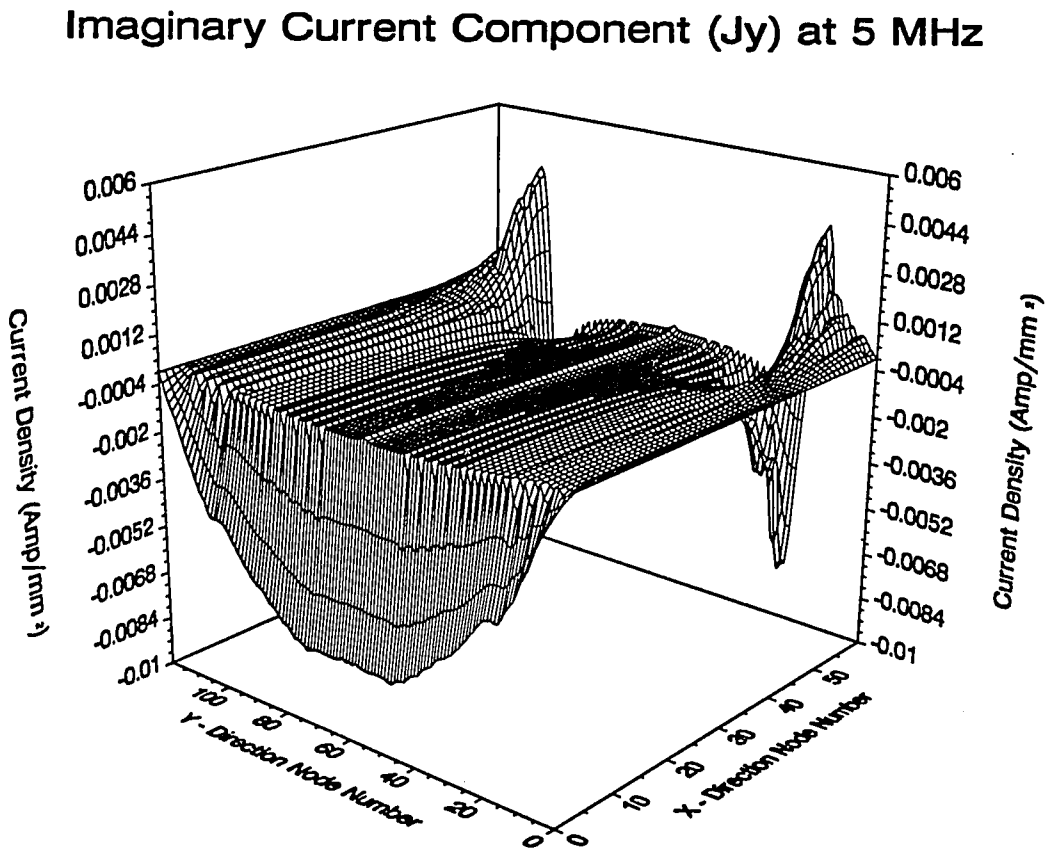

FIGURE 29: Imaginary current component (Jy) at 5 MHz

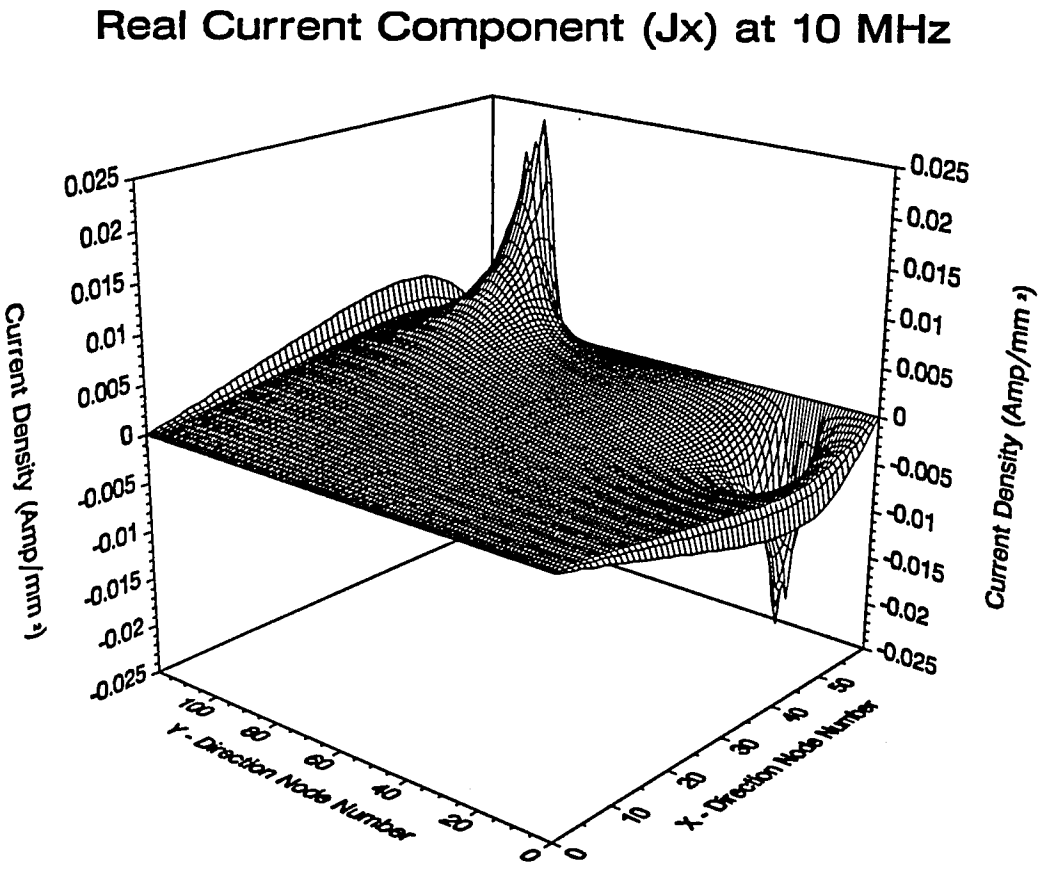

FIGURE 30: Real current component (Jx) at 10 MHz

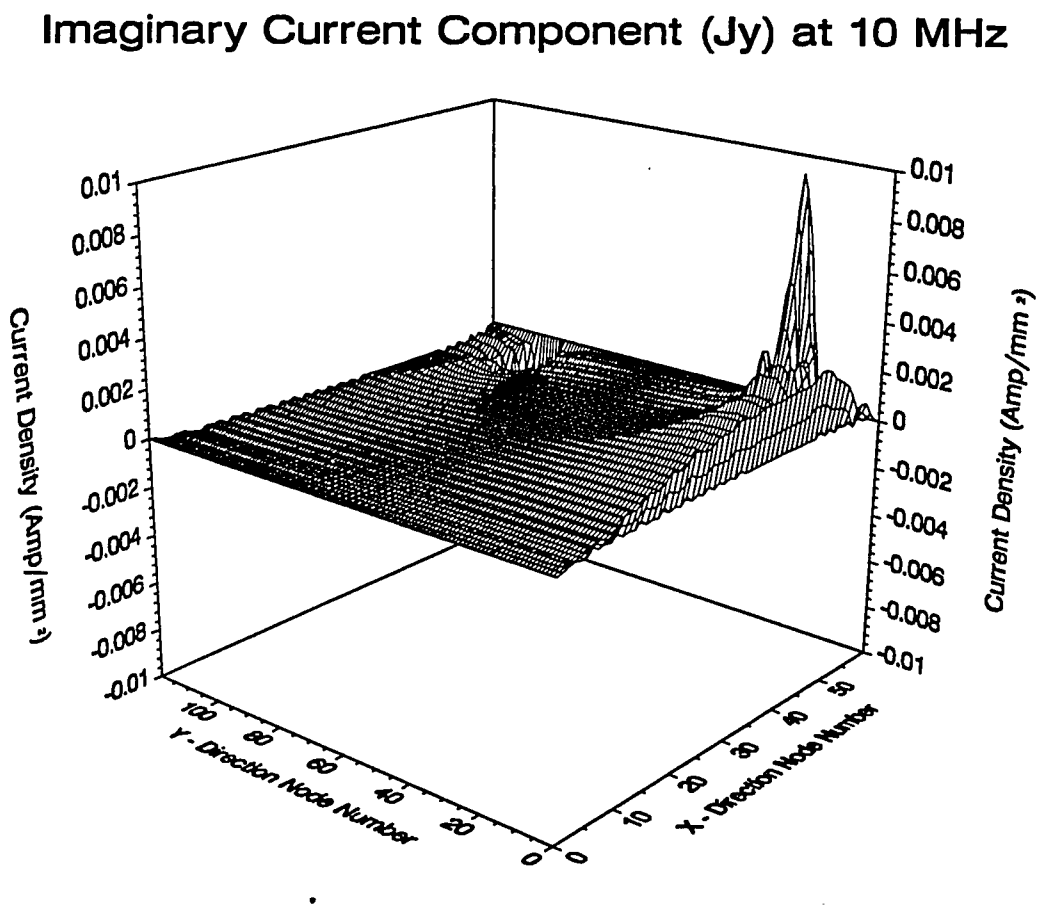

FIGURE 31: Imaginary current component (Jx) at 10 MHz

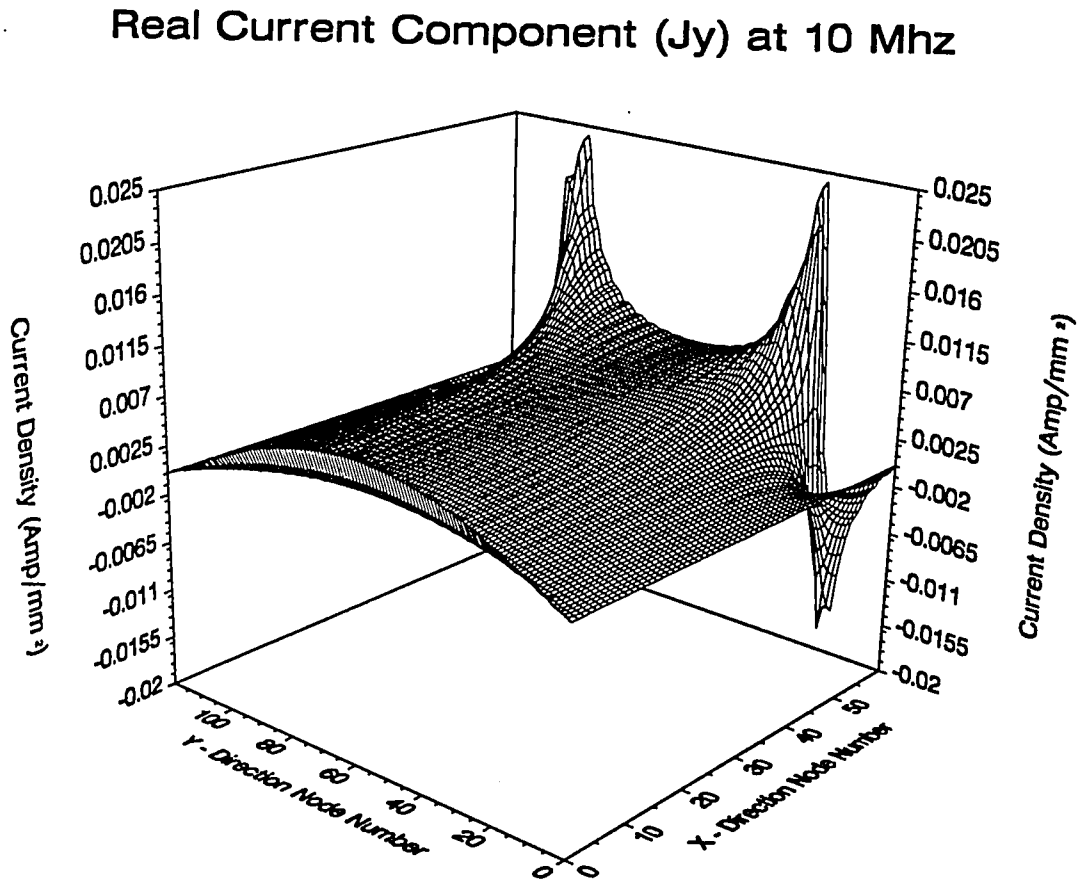

FIGURE 32: Real current component (Jy) at 10 MHz

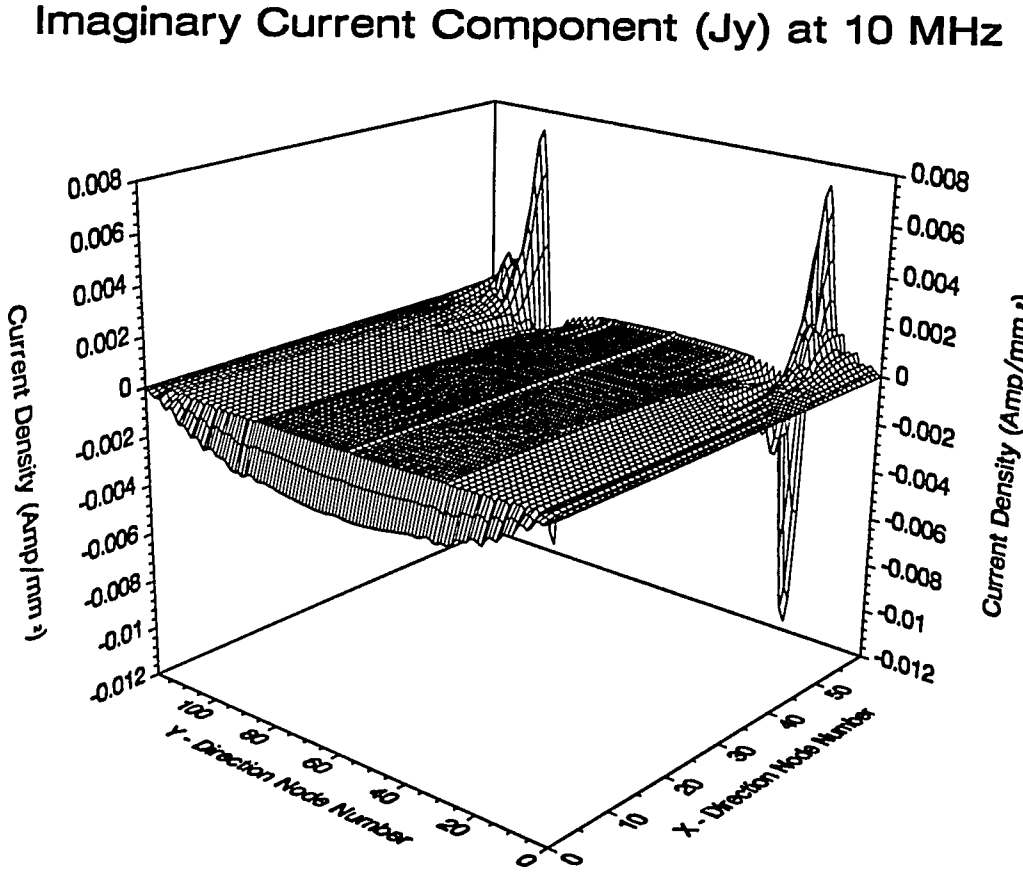

FIGURE 33: Imaginary current component (Jy) at 10 MHz

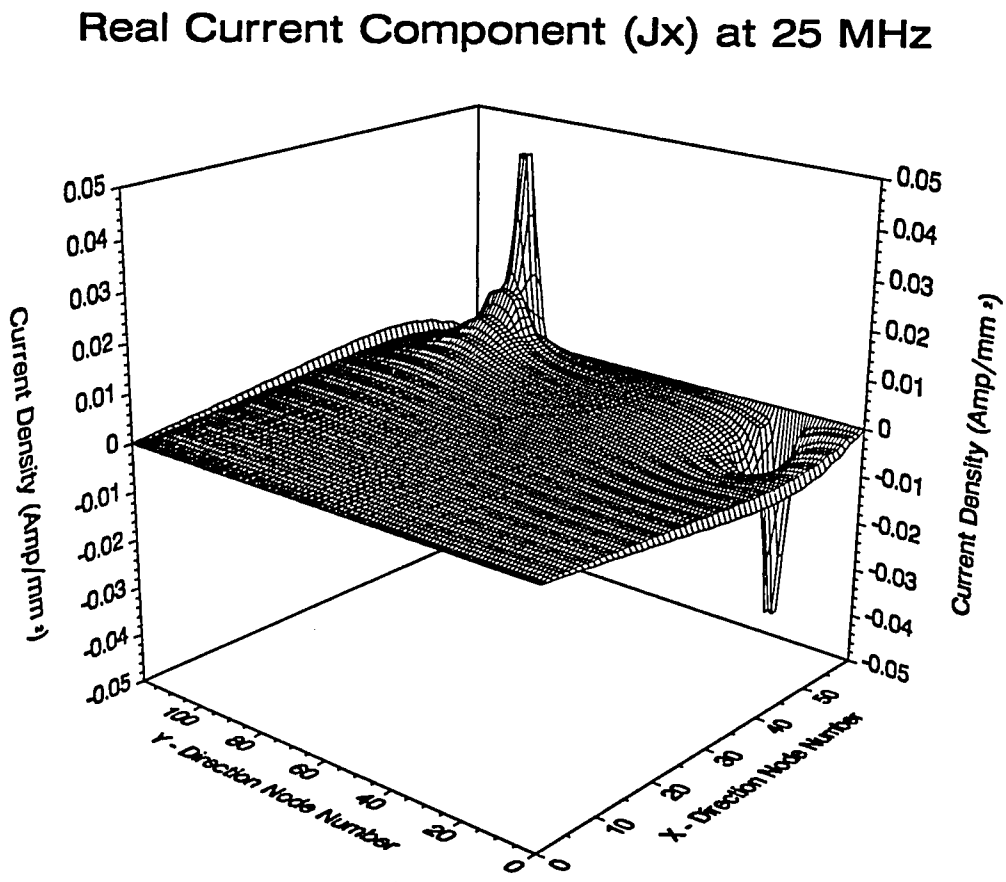

Figure 34: Real current component (Jx) at 25 MHz

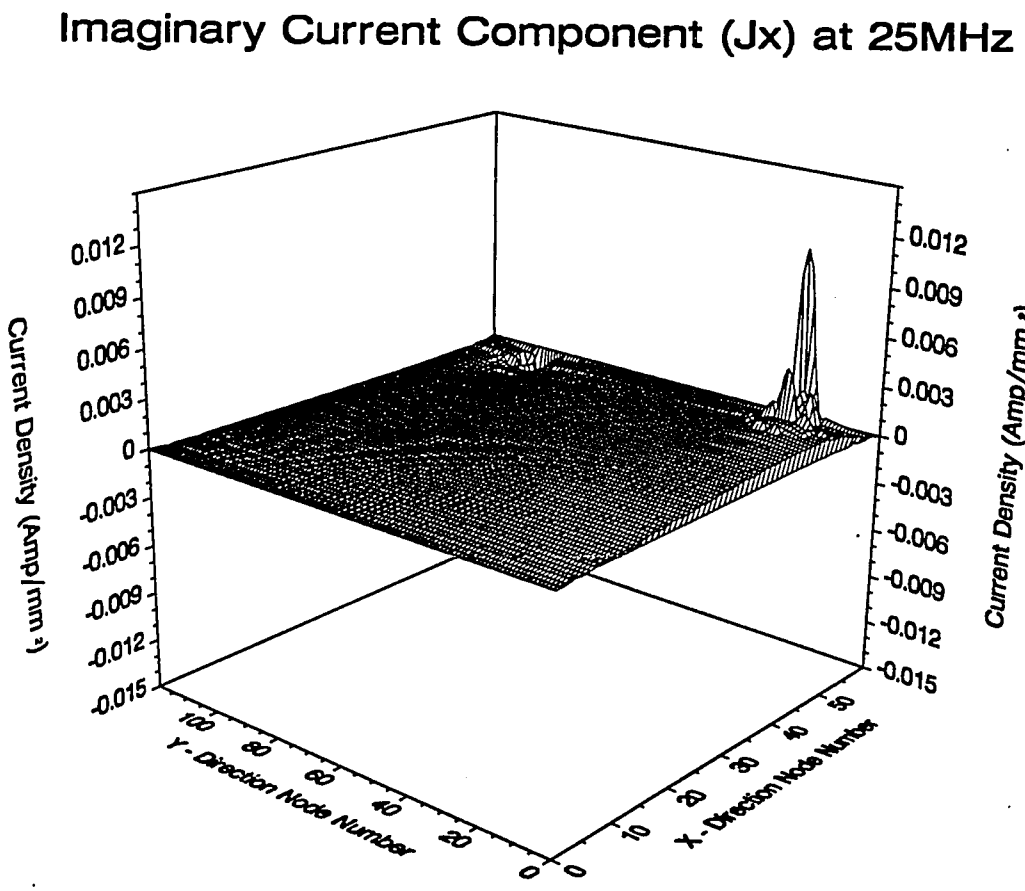

FIGURE 35: Imaginary current component (Jx) at 25 MHz

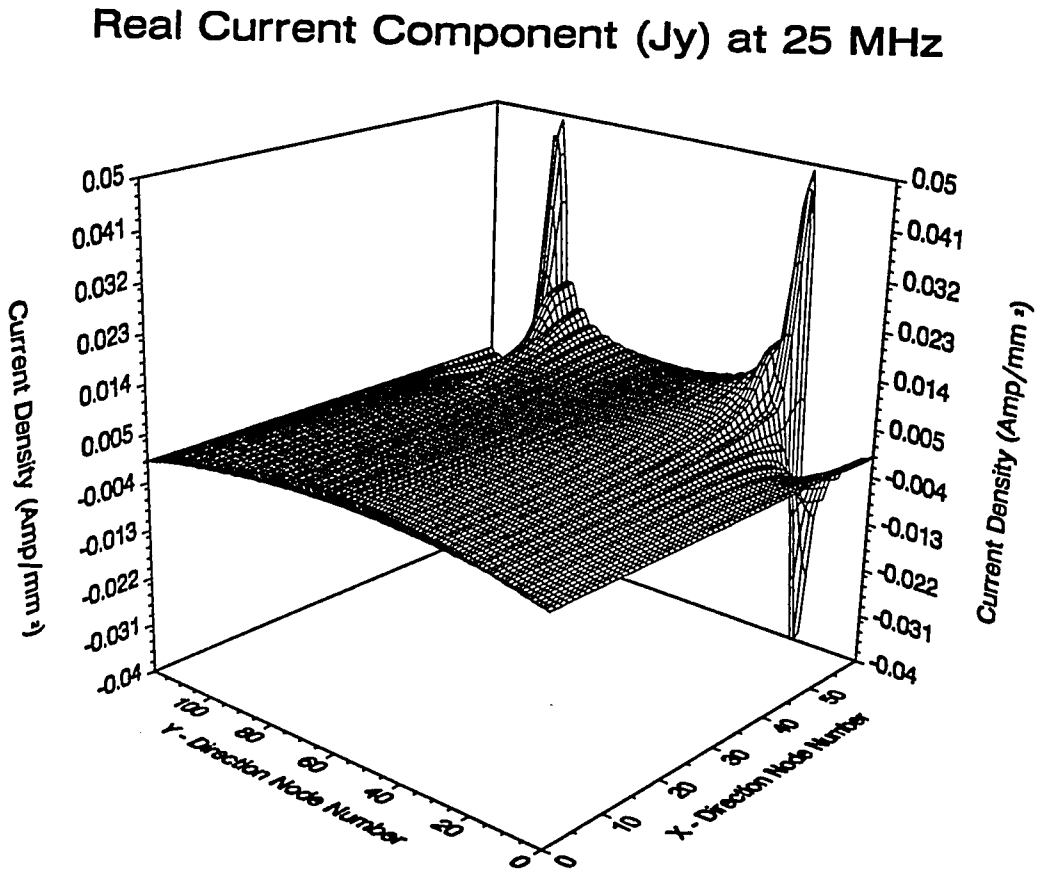

FIGURE 36: Real current component (Jy) at 25 MHz

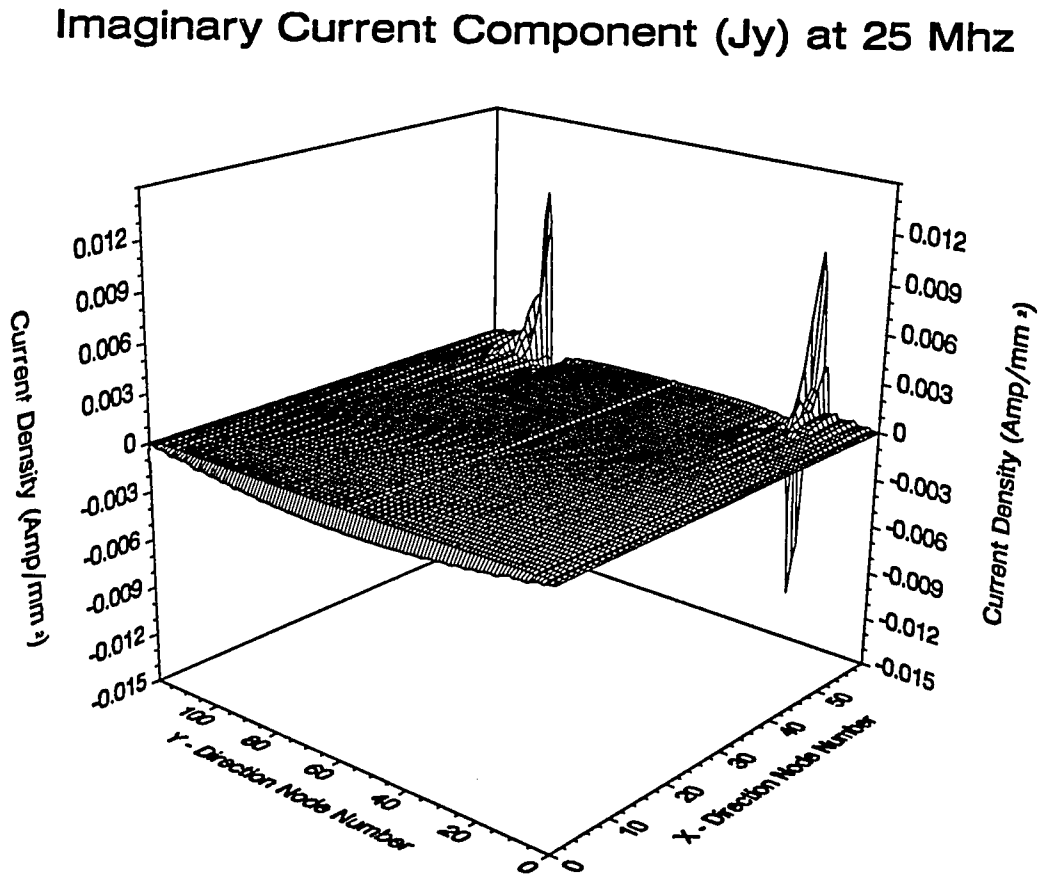

FIGURE 37: Imaginary current component (Jy) at 25 MHz

As can be seen from the plots, the current flows away from the source towards the sink. The y current components have peaks close to the source and the sink which have opposite signs depending wether the current is flowing along the positive or negative y direction. The same statement can be made about the x current components. The appearance of these peaks in the plots gives some justification to the correctness of the current distribution. Let us now look at the plots for the plane with perforation(shown in figure 38 below):

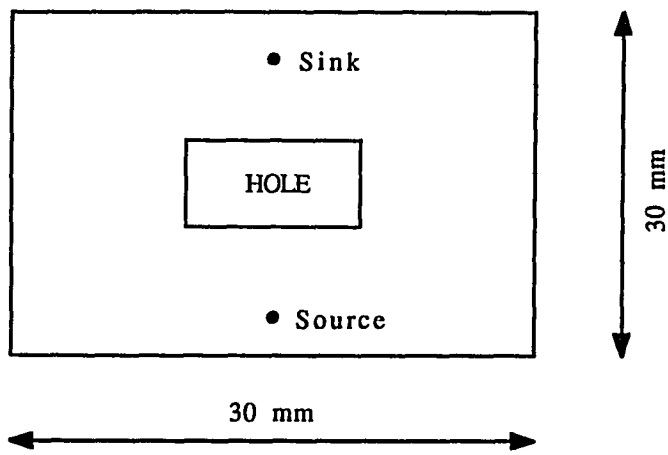

THICKNESS: 1.0 mm
CONDUCTIVITY: 58.0 mho/mm
PERMEABILITY: 12.56E-10 H/mm

HOLE LOCATION: LOWER LEFT CORNER X = 10, Y = 10
UPPER RIGHT CORNER X = 20, Y = 20

SOURCE LOCATION: X = 15, Y = 5
SINK LOCATION: X = 15, Y = 25

FIGURE 38: Plane with perforation

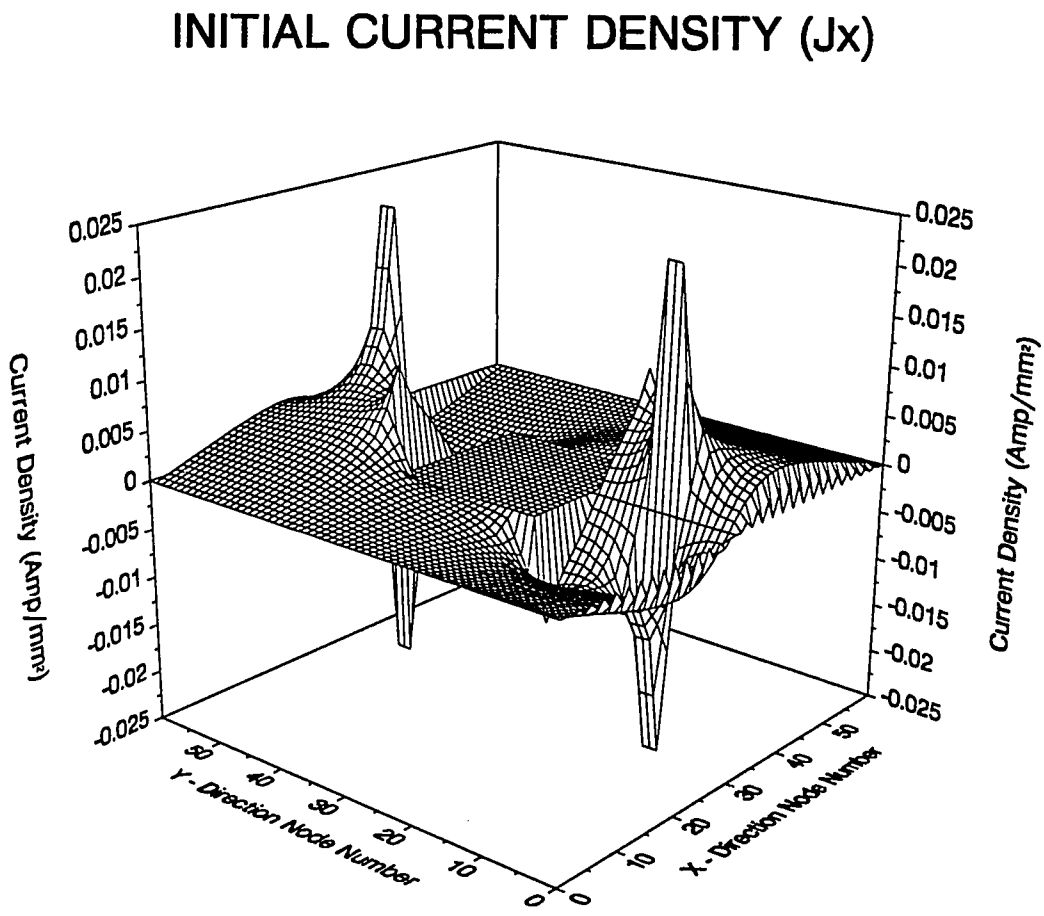

FIGURE 39: Initial current component (Jx) at DC

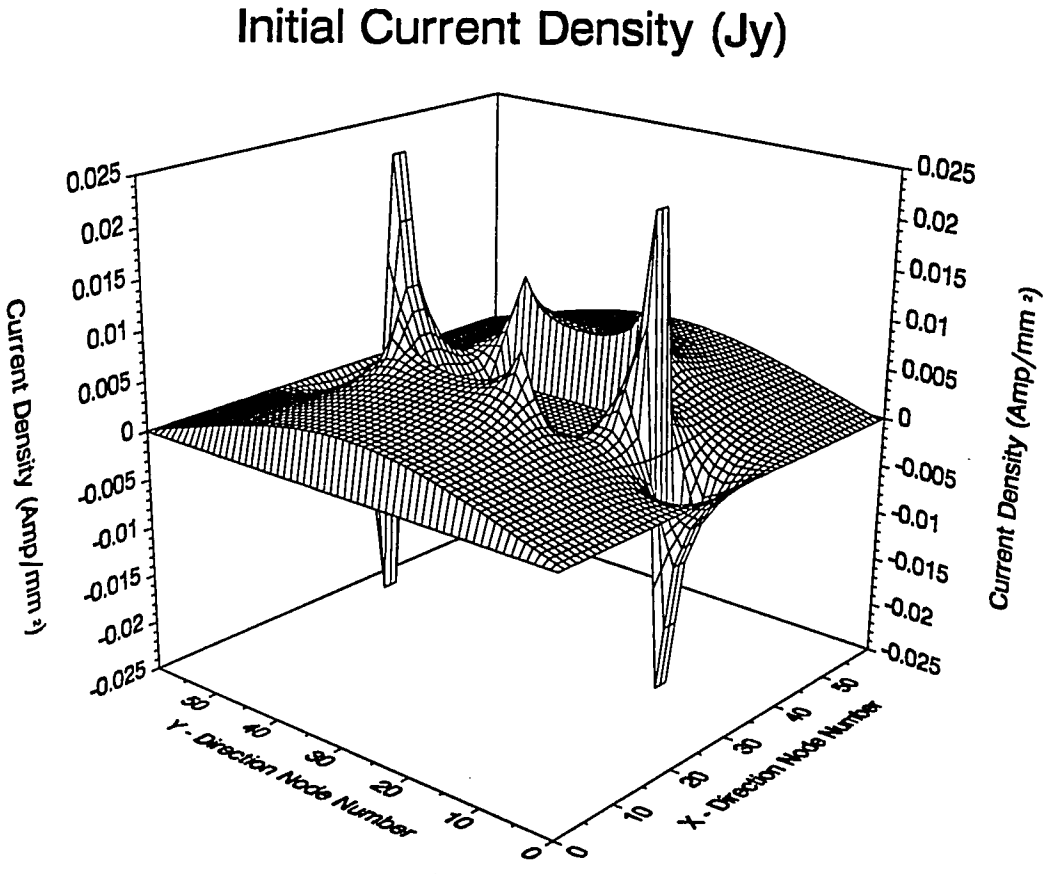

FIGURE 40: Initial current component (Jy) at DC

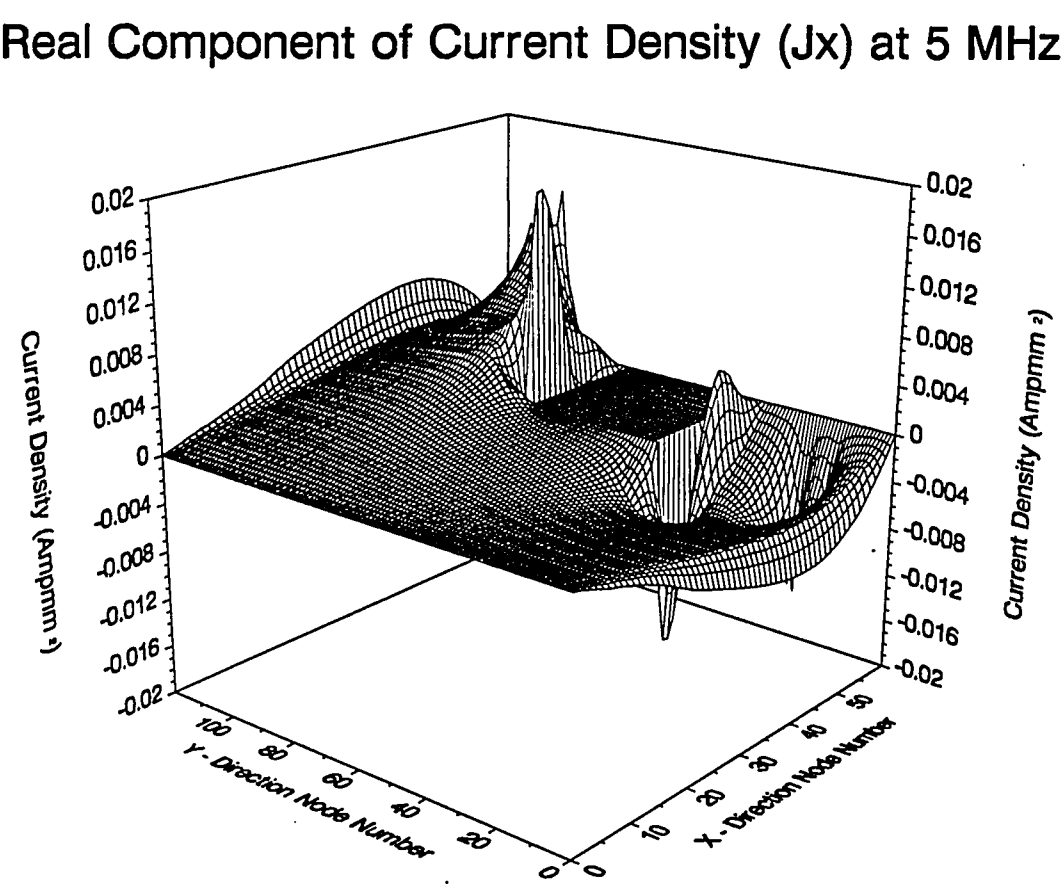

FIGURE 41: Real current component (Jx) at 5 MHz

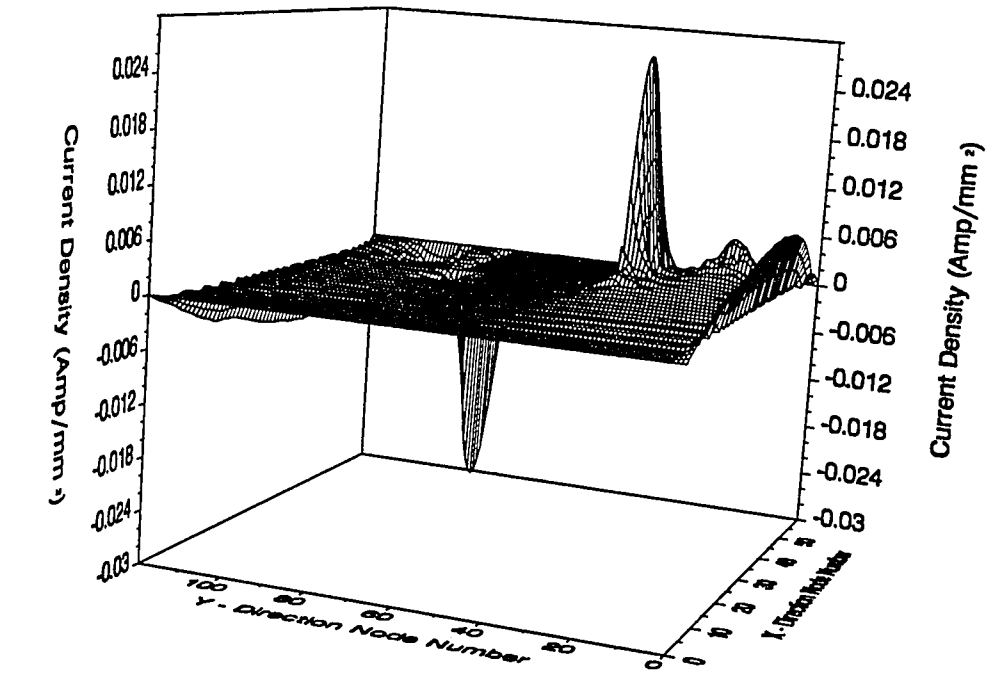

FIGURE 42: Imaginary current component (Jx) at 5 MHz

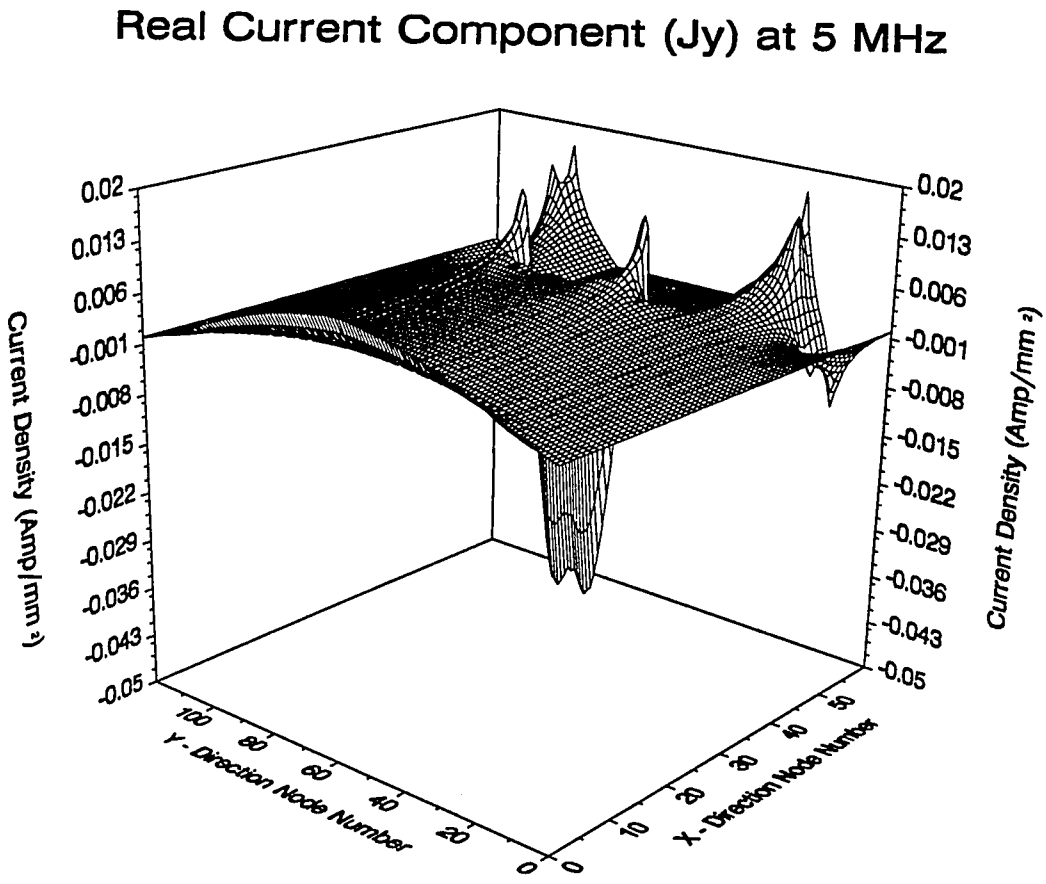

Figure 43: Real current component (Jy) at 5 MHz

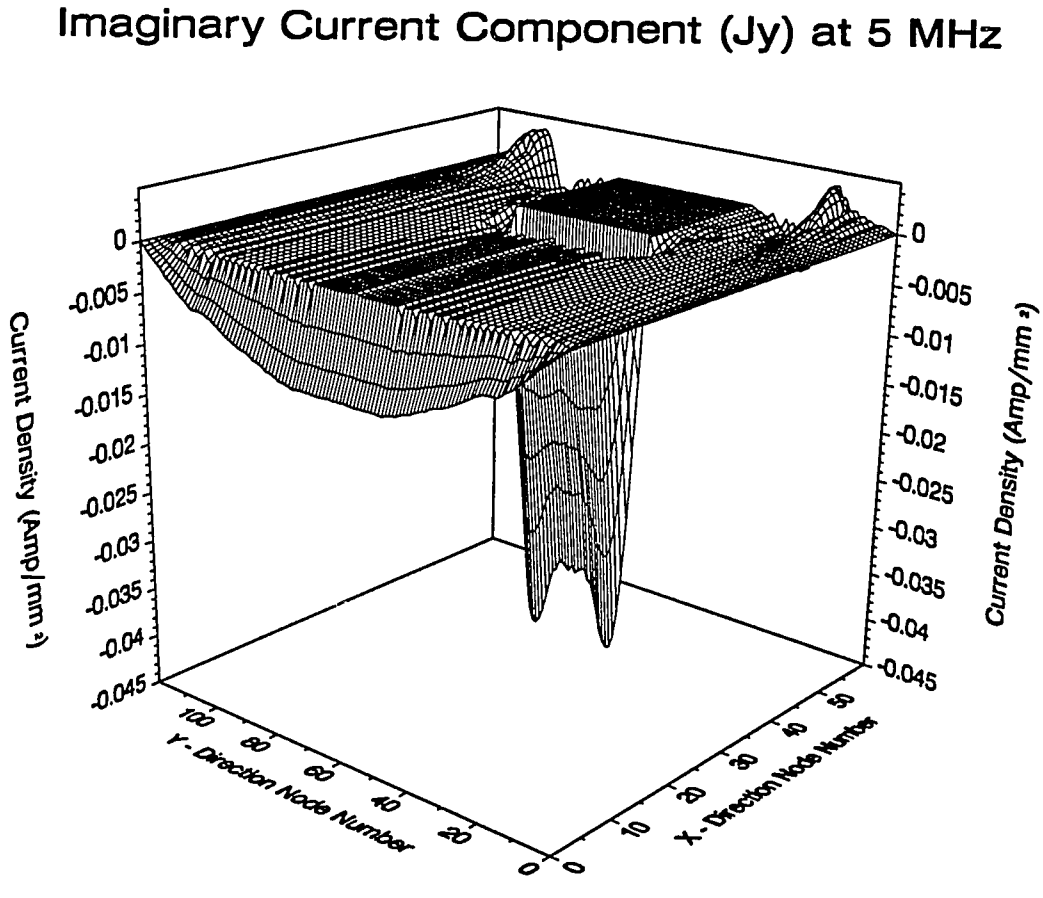

FIGURE 44: Imaginary current component (Jy) at 5 MHz

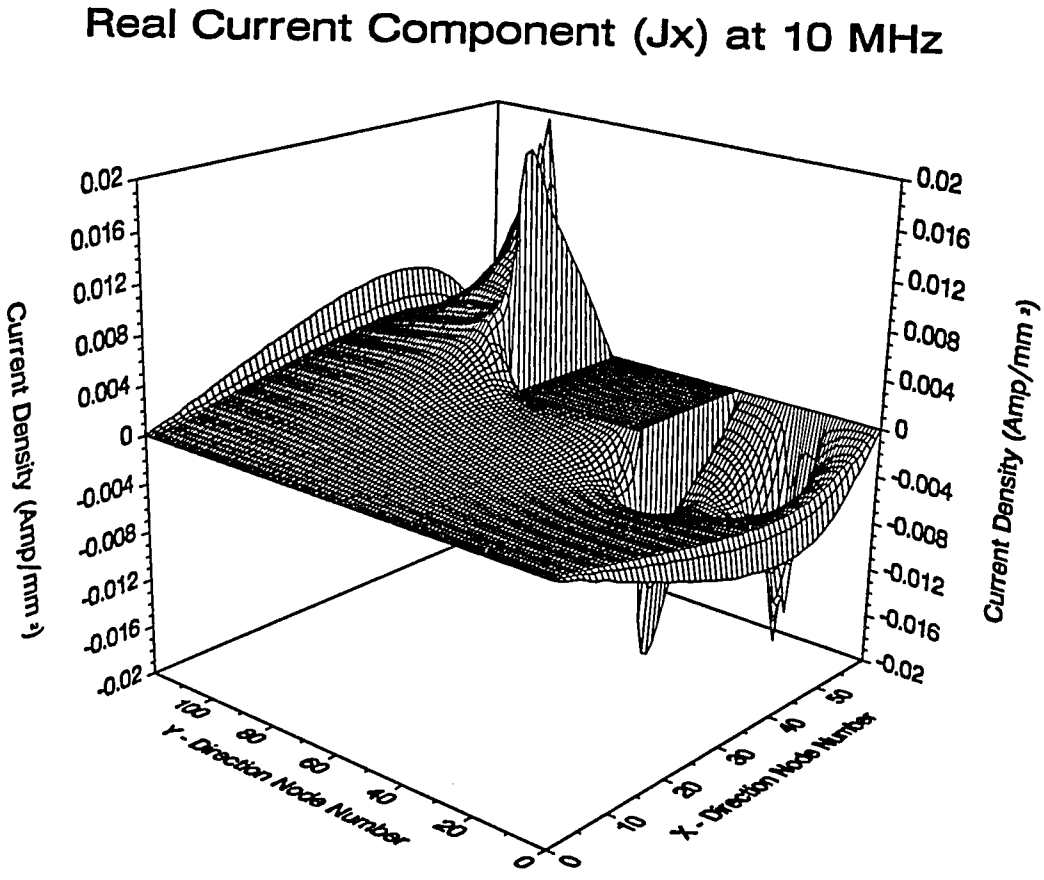

FIGURE 45: Real current component (Jx) at 10 MHz

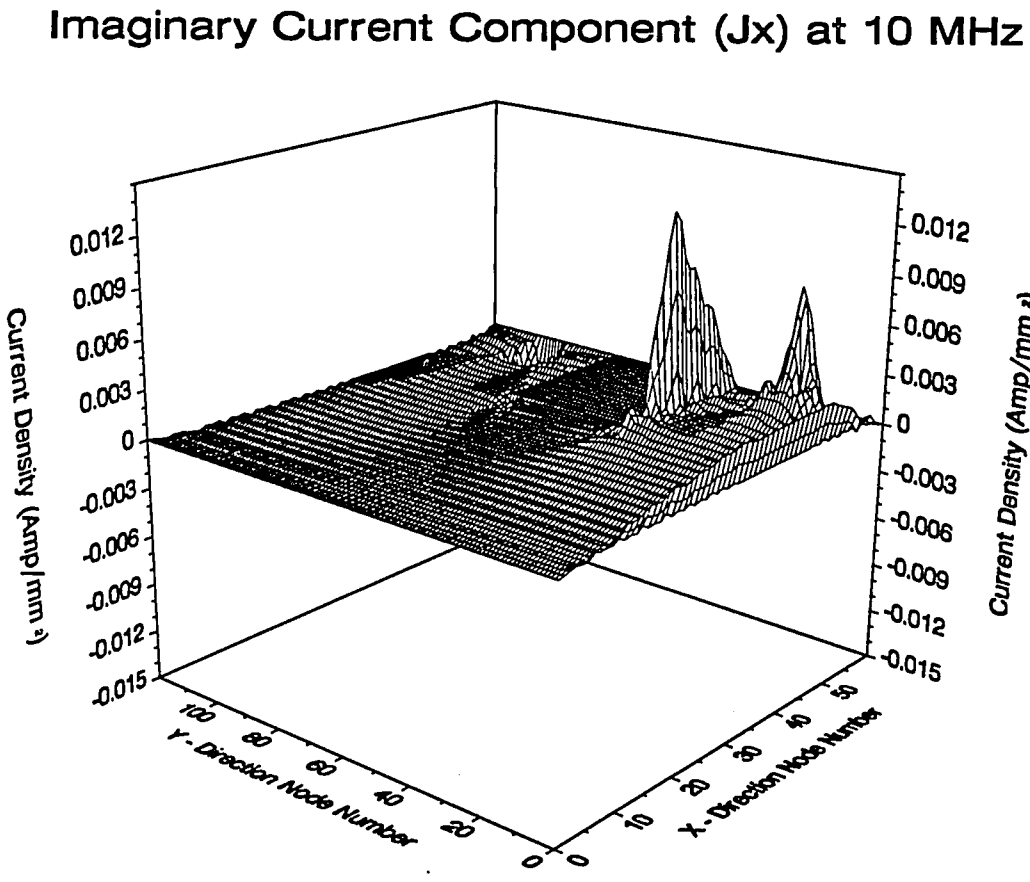

FIGURE 46: Imaginary current component (Jx) at 10 MHz

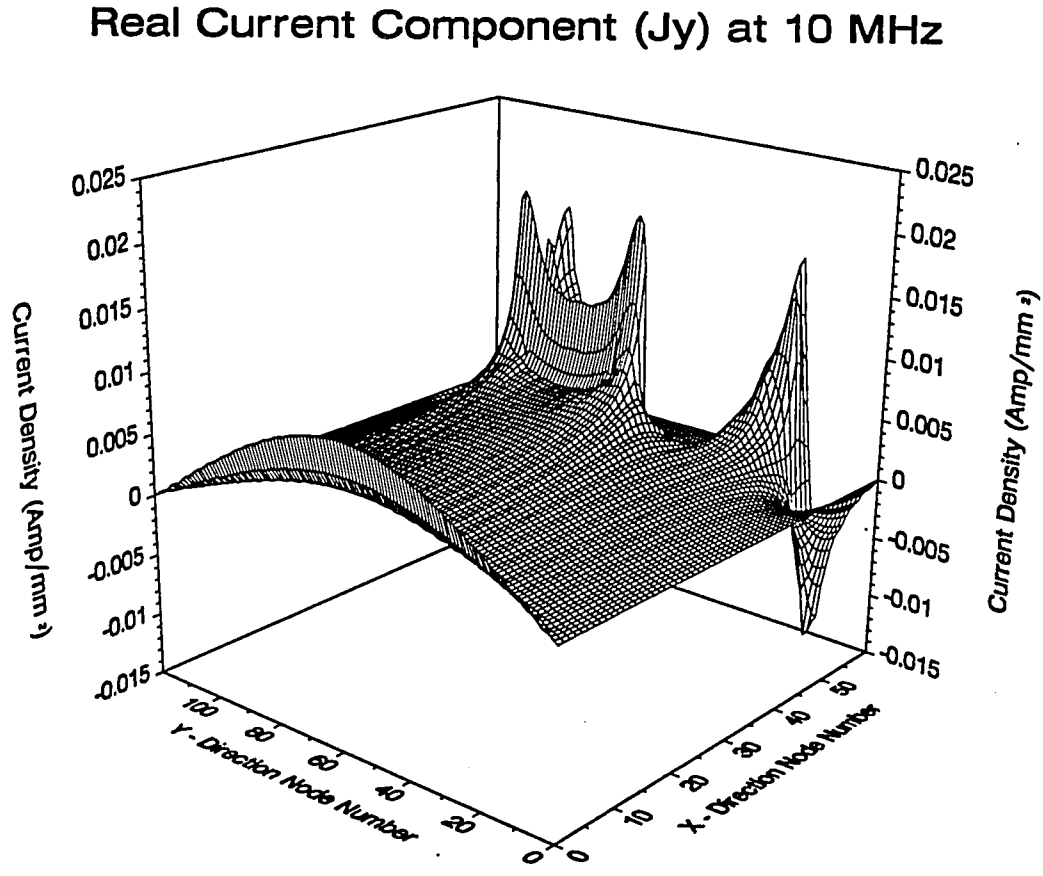

FIGURE 47: Real current component (Jy) at 10 MHz

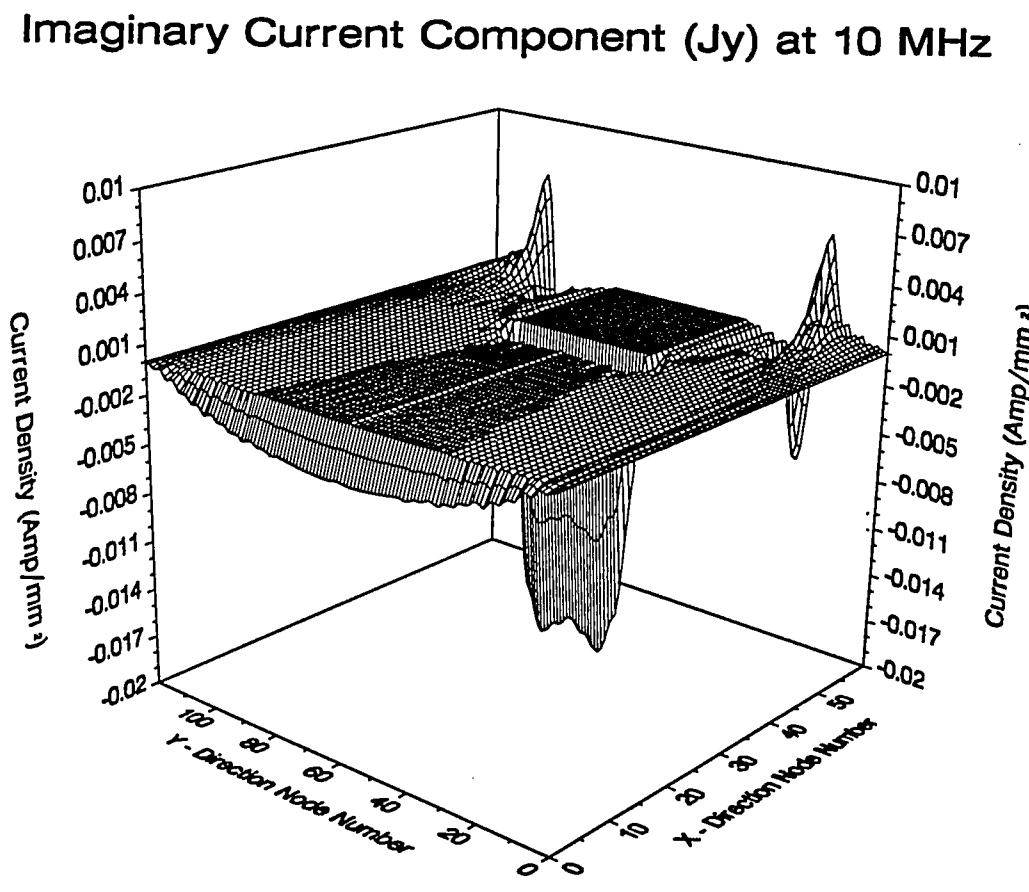

FIGURE 48: Imaginary current component (Jy) at 10 MHz

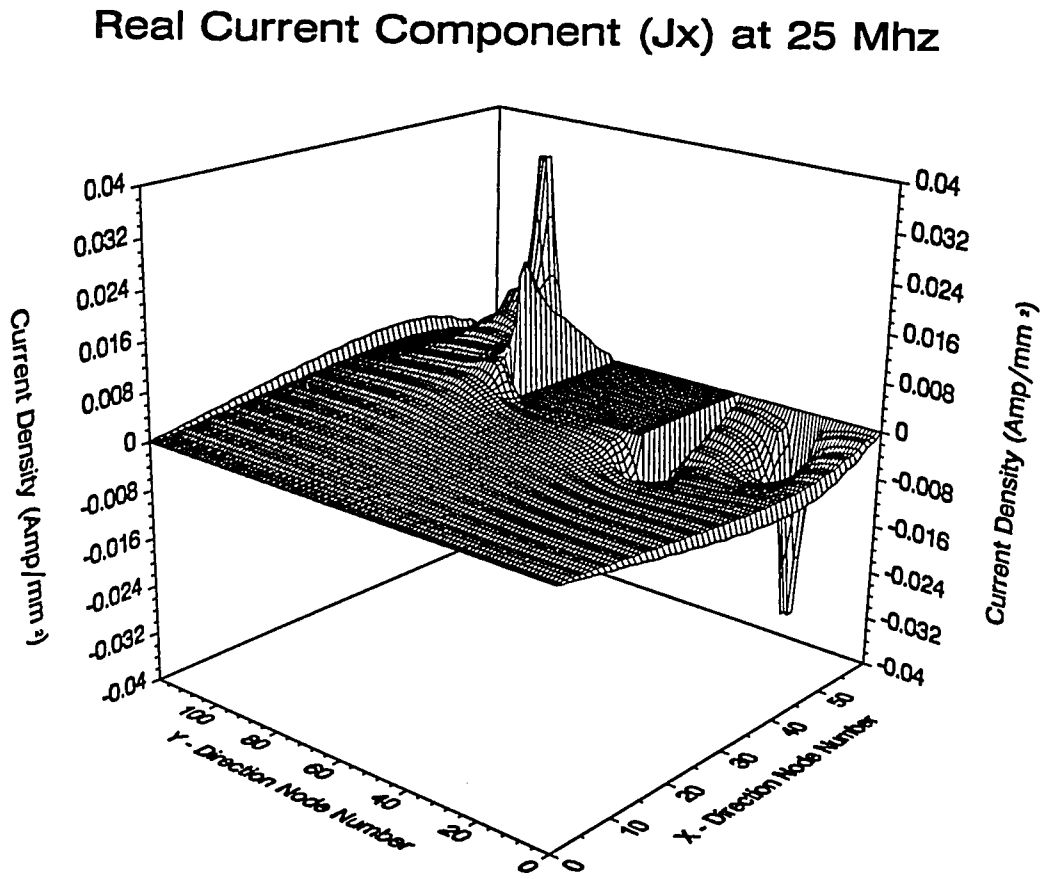

Figure 49: Real current component (Jx) at 25 MHz

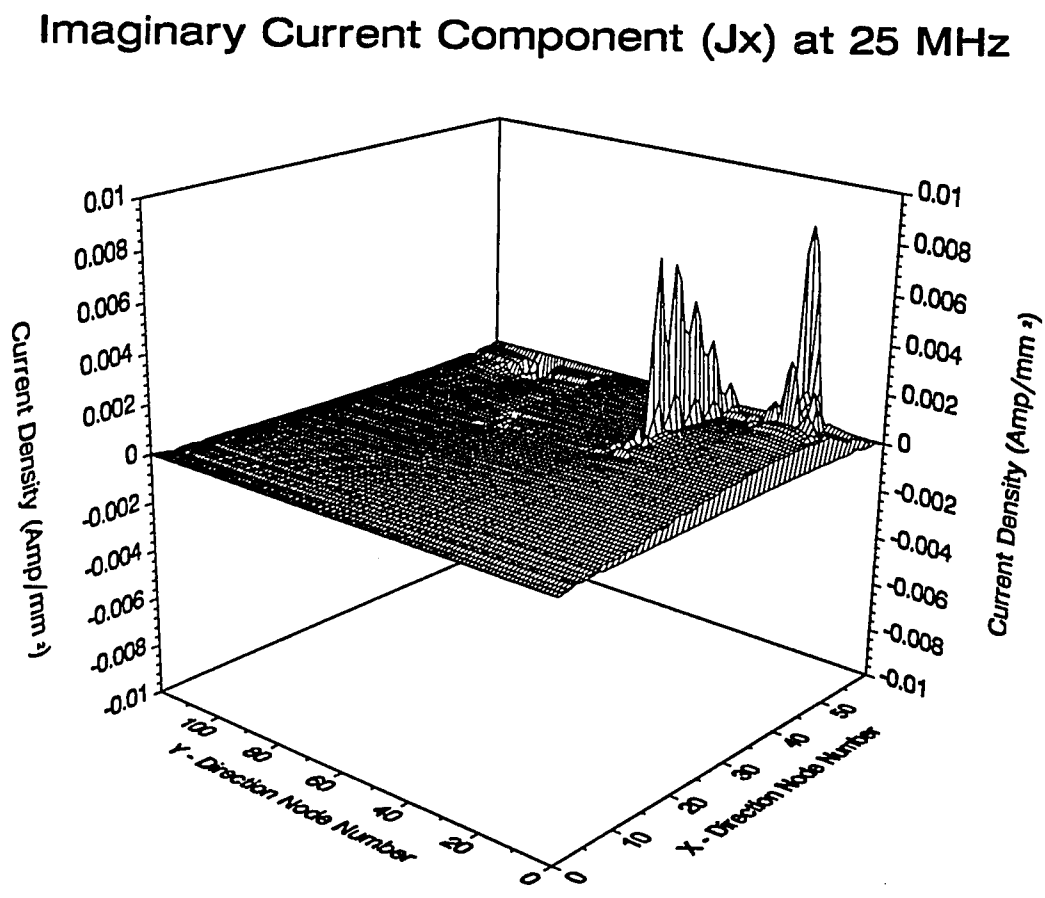

FIGURE 50: Imaginary current component (Jx) at 25 MHz

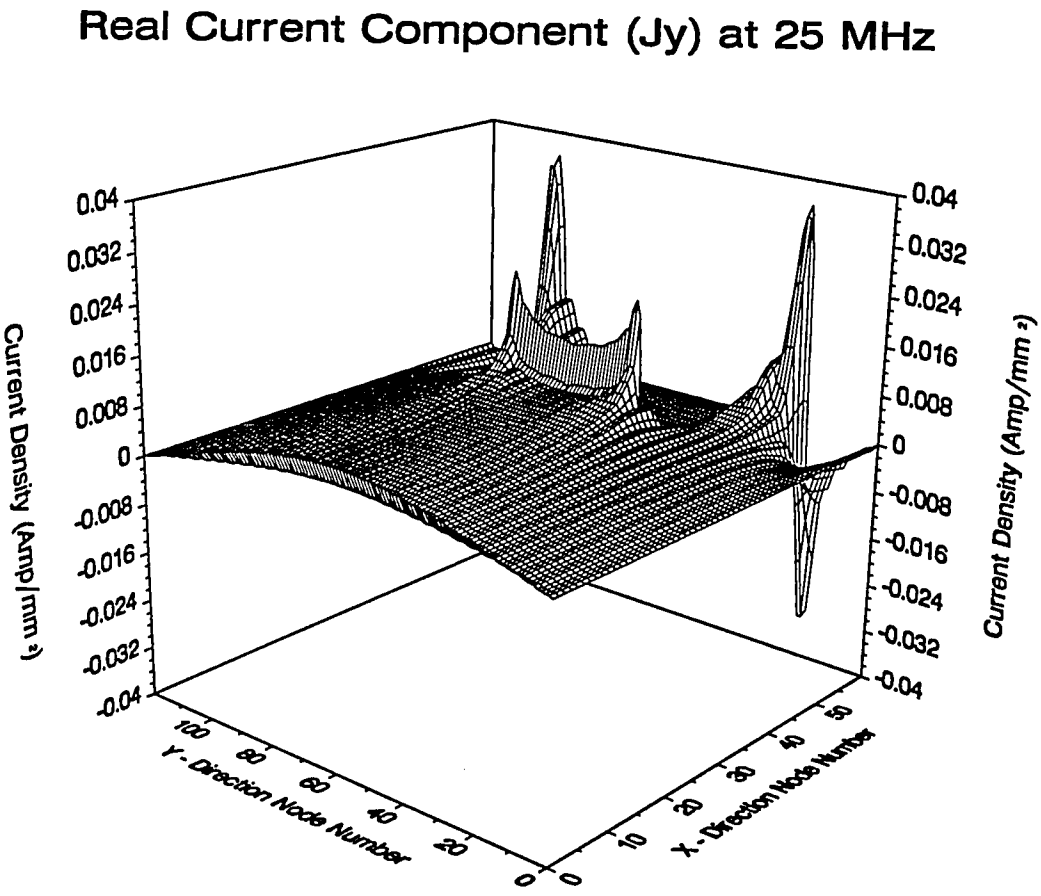

FIGURE 51: Real current component (Jy) at 25 MHz

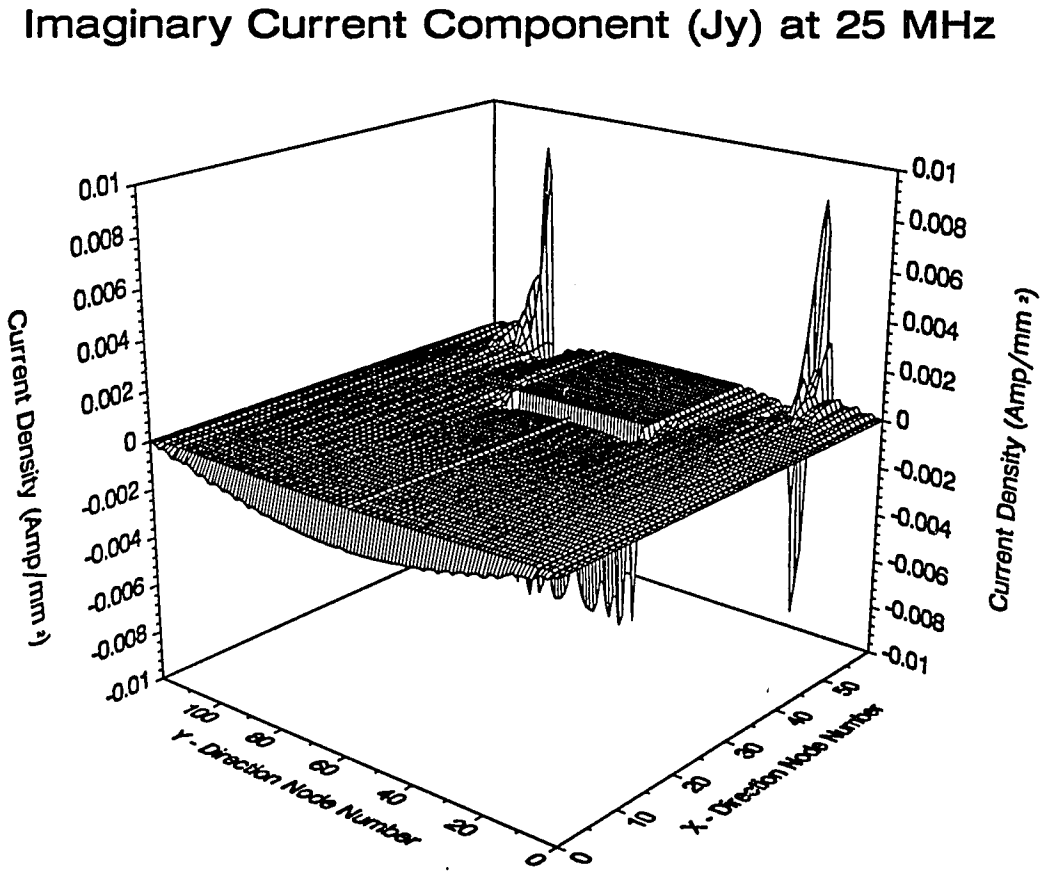

FIGURE 52: Imaginary current component (Jy) at 25 MHz

The procedure used to calculate 'A' (the magnetic vector potential) is not accurate and therefore, the inductance values obtained for ground planes are not correct. The magnetic vector potential was calculated from equation:

$$\bar{J}_{ac} = -\sigma\nabla\phi - j\omega\sigma\,\bar{A} \quad \text{where } '-\sigma\nabla\phi' \text{ is approximated as } \bar{J}_{dc}$$

and 'A' can be written as:

$$\bar{A} = 1/j\omega\sigma(\,\bar{J}_{dc} - \bar{J}_{ac})$$

A possible explanation for the numerical performance of this equation is that in the dynamic case, as ω increases the term $j\omega\sigma\,\bar{A}$ tries to counteract the term $-\sigma\nabla\phi$ and lead to the anticipated result $\bar{E} \rightarrow 0$ inside a good conductor. The 'A' should be calculated using $\bar{J}_{ac}$ only and by integrating over every grid in the plane. The approximation of ' ϕ ' in the above equation by it's DC value brings in the inaccuracy in the inductance values. The potential ' ϕ ' should be calculated at the frequency of operation if this methodology is to be successfully implemented.

The plane conductivity is 58.0 mho/mm and the permeability 12.56e-10 H/mm. The chosen value of conductivity is not realistic and is 1000 times less that of copper. This had to be done due to memory limitations imposed by the required array sizes for the approximate problem for the case of actual copper. Since the discretization is dictated by the skin depth, the extremely low values of skin depth at high frequencies result in very fine grids for problems of practical interest.

The table below shows the inductance values obtained for the geometry of Figure 23 at different frequencies.

Frequency	Inductance
DC	16.10 nH
1 MHz	0.465 nH
5 MHz	0.140 nH
10 MHz	0.046 nH
25 MHz	0.01 nH

From these values it is clear the 'A' is not calculated accurately using the proposed approach.

As discussed earlier, the accuracy of the calculated current distribution is dependent on the plane discretization and varies with varying discretization. Obviously, this dependence also impacts the accuracy of the calculated resistance values.

Some general rules can be applied to select values for plane discretization based on the skin depth at the frequency of operation.

1) The DC resistance value obtained from UALGRL should be an accurate value obtained after experimenting with different discretizations.

2) For the frequency-dependent case, it is essential that the grid size be at least "skin depth/4" for lower frequencies (i.e. 500 KHz, 1MHz) and increase to "skin depth/8" for higher frequencies (i.e. 5 MHz, 25 MHz, 50 Mhz) to get reasonably accurate current values and resistance values.

3) However, since the initial current distribution is obtained by interpolation from the DC distribution calculated using UALGRL, it is important to use these limits on the grid size for the frequency-dependent case to guide the selection of the grid size for UALGRL. In other words, the grid size for UALGRL should not be much larger than that for the frequency dependent case.

The results obtained for the two cases of Figure 23 and Figure 38 are tabulated below:

For the geometry of Figure 23: (plane without perforation)

Frequency	Resistance	Skin depth	$\Delta x = \Delta y$
DC	0.028 ohm		30 mm
1 MHz	0.018 ohm	2.08 mm	0.5 mm
5 MHz	0.021 ohm	0.93 mm	0.25 mm
10 MHz	0.022 ohm	0.66 mm	0.125 mm
25 MHz	0.024 ohm	0.41 mm	0.0625 mm
50 MHz	0.025 ohm	0.29 mm	0.025 mm

For a plane with perforation (Figure 38) the resistance values are:

Frequency	Resistance	Skin depth	$\Delta x = \Delta y$
DC	0.037 ohm		30 mm
1 MHz	0.045 ohm	2.08 mm	0.5 mm
5 MHz	0.086 ohm	0.93 mm	0.25 mm
10 MHz	0.054 ohm	0.66 mm	0.125 mm
25 MHz	0.039 ohm	0.41 mm	0.0625 mm
50 MHz	0.177 ohm	0.29 mm	0.025 mm

The resistance values are sensitive to the choosen discretization and this is illustrated in the table below: (for figure 38) plane with perforation.

Frequency	$\Delta x = \Delta y$	Resistance
5 MHz	0.5 mm	NaN
	0.25 mm	0.086 ohm
	0.125 mm	0.035 ohm
	0.0625 mm	0.033 ohm

→ Non convergent

SKIN DEPTH = 0.934mm

The same behavior of resistance can be seen for figure 23 (plane without perforation) and is shown below:

Frequency	$\Delta x = \Delta y$	Resistance
1 MHz	1.0 mm	NaN
	0.5 mm	0.018 ohm
	0.25 mm	0.019 ohm
	0.2 mm	0.031 ohm
	0.125 mm	0.021 ohm
	0.0625 mm	0.023 ohm

→ NON CONVERGENT

SKIN DEPTH = 2.08mm

We can now evaluate the effectiveness this method of computing the frequency dependent current distribution in a ground plane and the plane parasitics based on our observations:

* The accuracy of the numerical method is very sensitive to the choice of the grid size which prevents the reliable calculation of the current density. This further effects the accuracy of the resistance and inductance values computed using this method.

* It cannot be applied towards solving practical problems due to memory constraints caused by very fine grid sizes required for practical frequencies of interest. The plane used to do the actual simulations has a conductivity equal to 1/1000 that of copper. If the actual conductivity of copper is used, the grid sizes that need to be solved at frequencies of interest for the geometry of Figure 23 are:

Frequency	Skin depth	Discretization	Grid size
500 KHz	0.092 mm	0.01 mm	3000 by 3000
1 MHz	0.06 mm	0.005 mm	6000 by 6000
10 Mhz	0.02 mm	0.002 mm	15000 by 15000
50 Mhz	0.0092 mm	0.001 mm	30000 by 30000

A look at these numbers shows how difficult it can get to compute the current distribution in the plane.

CHAPTER 4

4.1 Conclusions

An iterative finite differencing technique was utilized to solve the two dimensional diffusion equation for the current distribution on the ground plane. The initial DC distribution was obtained from UALGRL by utilizing an interpolation technique and the frequency dependent current distribution was then obtained by imposing the necessary boundary conditions and allowing the current to redistribute itself over the plane. Finally, the plane parasitics were computed using integral methods and energy considerations. The conclusions that can be drawn from this methodology are as follows:

1) The current density as calculated by the aforementioned method is sensitive to the chosen plane discretization and can vary depending on the chosen value. At a particular frequency, the discretization is linked to the skin depth, and therefore, the increase or decrease in discretization will indicate the effective change in the current distribution from its value at a lower frequency. The increase in discretization with frequency can be identified as an increase in the sampling rate of the current on the plane.

2) The accuracy of the current values is also effected by the iterative technique; namely, the way the iteration is performed. A wrong method can lead to misleading impressions on the physical nature of the problem, by the erroneous current values on a particular side of the plane.

lead to misleading impressions on the physical nature of the problem, by the erroneous current values on a particular side of the plane.

3) The current distribution on the plane does not seem to be changing a lot from its DC distribution for frequencies up to 50 MHz (the highest frequency used) for a plane with no hole at least for the values of conductivity used in our examples. However, the current distribution seems to get distorted by the presence of the hole as can be seen in the plots for this case.

4) The magnetic vector potential 'A', should be computed using the total current ($\bar{J}_{ac}$) rather than the difference of the AC and DC current as done in this method. Although this method is extremely fast computationally, it does not provide the accuracy needed for the reliable computation of the magnetic vector potential.

5) The variation in the calculated current values has an impact on the resistance values for the plane which can vary accordingly. The relationship between dx, dy and the current distribution results in varying resistance values at different frequencies corresponding to different discretizations. However, as illustrated in the results, at a particular frequency, lower discretization values lead to less variation in the resistance values.

Appendix A

3.1 Program Execution:

There are two versions of the program that compute the frequency dependent current distribution for a ground plane and a third program that computes the resistance and inductance of a ground plane. However, the inductance value is not correct and should not be utilized for any modeling.

The following points should be kept in mind while running both the programs to compute the frequency dependent current distribution on a ground plane.

1) The discretization used while running UALGRL i.e. ("dx" and "dy"), should be integer multiples of the discretization used while running this program. For example:

if dx = 0.125e-2 and dy = 0.2e-2 (UALGRL dimensions are in metres).

then delta-x = .25mm is correct because 0.25 * 5 = 1.25mm.

and delta-y = 1.0mm is correct because 1.0 * 2.0 = 2.0mm.

2) The choosen discretization distance should be approximately less than or equal to: " skin depth" / 4. However, as frequency increases this distance moves towards " skin depth" / 8 in order to get accurate results.

3) The input file from UALGRL should be called "dppot.in". This can be changed by changing the name in the source code, if desired.

4) All dimensions used should be in "mm".

5) The program recognizes the presence of a hole by a "1" and a "0" tells the program that no hole is present.

6) The convergence parameter should lie within the range $1 < a < 2$.

7) The coordinates for the hole origin and the hole width and length should be entered in terms of integers. For ex: if the hole is located in UALGRL by the following coordinates left bottom: 0.125e-2, 4.0e-2

right bottom: 0.375e-2, 6.0e-2 (both are in metres)

Then for a delta-x = 0.25mm and delta-y = 1.0mm, the hole origin is specified as

hole origin: 5, 40 because 1.25/0.25 = 5 and 40/1 = 40.

Similarly the width of the hole = 2.5/0.25 = 10 and length = 20/1 = 20.

8) This program can handle any number of grid points required to compute the frequency dependent current distribution, as long as memory is not a problem.

9) The two versions of this program have different output formats. One version prints the output for the "x" current component column wise starting with the column x = 0. This is shown in figure 20 below. The output consists of

the real and imaginary current components, current magnitude, coordinates of the point and the iteration at which the point converges.

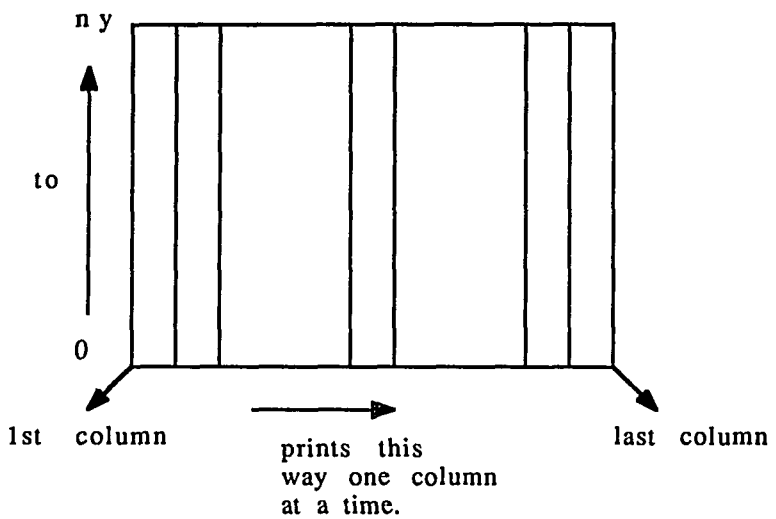

FIGURE 53: Printing format for x component

10) The output for the "y" current component is printed row wise starting with the first row y = 0. This is shown in figure 21 on the next page. It's output format is same as described for the x-component.

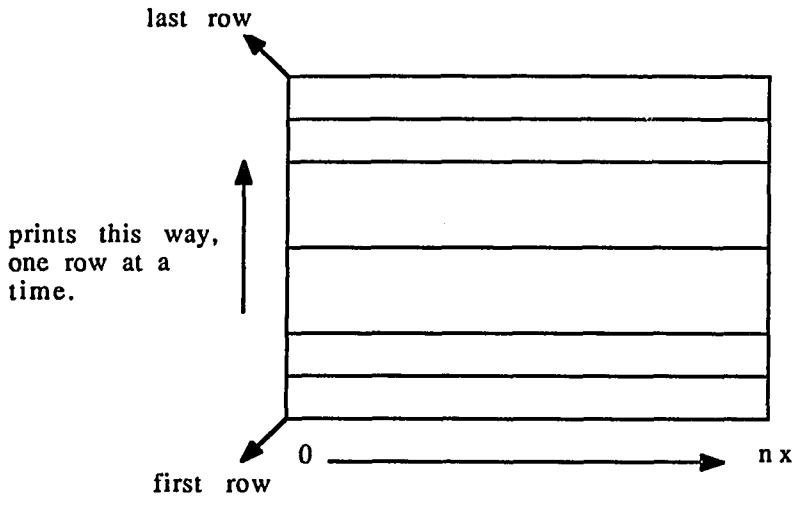

FIGURE 54: Printing format for y component

11) This version also prints the initial "x" and "y" current components which are basically the DC values obtained after interpolating the output file from UALGRL. These files are called "initjy.dat" and "initjx.dat".

12) The other version of the program prints every desired row (i.e. every n^{th} row) and the real and imaginary values of the "x" and "y" components in that row. The value of these points is also printed. The output file is called "out".

13) The program that calculates the resistance of a ground plane has exactly the same input file format.

APPENDIX B

The program to compute the frequency dependent current distribution or the resistance and inductance of a plane can be run interactively or by specifying an input file. The command to do this is illustrated below:

"program.exe <in.dat>out"

A sample input file is also shown below: Please refer to section 3.1 to learn how to execute the program.

5.0	Width (x-axis) of the plane (mm).
100	Length(y-axis) of the plane(mm).
0.25	Delta-x(mm).
1.00	Delta-y(mm).
100	Number of iterations.
1.011	Convergence Parameter.
0.001	Convergence Tolerance.
58.0	Conductivity(mho/mm).
1.0e6	Frequency(Hz).
4πe-10	Permeability.
1/0	1: Hole present, 0: Hole absent.
5	x-coordinate of hole origin.
40	y-coordinate of hole origin.
10	Width of hole.
20	Length of hole.
10	Print every tenth row.

For the resistance and inductance computation, the above shown input file remains the same except the last row, which is not used. A sample file of "dppot.in" is shown below: Let us assume that there are 10 rows in this file. Detailed instructions to run UALGRL are given in it's manual

First row	nx, ny	nx: Number of "x" divisions in the UALGRL grid.
		ny: Number of "y" divisions in the UALGRL grid.
Second row		Potential values starting from the first row or y = 0.
*		
*		
*		
Row seven		Last potential value.
Row eight		Total current in source/sink.
Row nine	dx, dy	dx: Discretization along x.
		dy: Discretization along y.
Row ten		Conductivity.

REFERENCES

[1] Press, H.W, Flannery, P.B, Teukolsky, A.S, Vetterling, T.W - "Numerical Recipes: The Art of Scientific Computing".

[2] Kenneth Huebner - "The Finite Element Method for Engineers", Engineering Mechanics Department, General Motors Research Lab.

[3] Lapidus, L, Pinder, F.G - "Numerical Solutions of Partial Differential Equations in Science and Engineering."

[4] Pasik, M, Cangellaris, A.C, Prince, J.L - "UALGRL, Power/Ground Plane Inductance and Resistance Calculator, User's Manual", The Center for Electronic Packaging, Department of Electrical and Computer Engineering, University of Arizona, Tucson, Arizona 85721.

[5] Blodgett, J. A - Microelectronic Packaging, Scientific American, pp 86-96, July 1983.

[6] Schmitt, M.A, Lam, K., Mosley, L.E, Choksi, G, Bhattacharya, B.K - Current Distribution in Power and Ground Planes of a Multilayer Pin Grid Array Package, Intel Corporation, Chandler, Arizona 85226.

[7] Cangellaris, A.C, Prince, J.L, Senthinathan, R - "Modeling of Power/Ground Plane Parasitics and Investigation of their contribution to the effective Inductance of VDD/VSS Chip Packaging Interface". Proceedings of the IEEE VLSI and GaAs Chip Packaging Workshop, P 32, October 1991.

[8] Tummala, Rao. R, Rymaszewski, J.E - Microelectronics Packaging Handbook.

[9] Wylie, C.R - Advanced Engineering Math.

[10] Voranantakul, S, Jones, C.R - Current Magnitude and Stremlines on a VLSI Ground Plane, Transactions of the Society for Computer Simulation, Vol 4, No 3, Page 225-268.

[11] Shrivastava, A.U, Lan Bui, B - Inductance Calculation and Optimal Pin Assignment for the Design of Pin Grid Array and Chip Carrier Packages, IEEE Transactions on Components, Hybrids, and Manufacturing Technology, Vol 13, No 1, March 1990.

[12] Senthinathan, R, Prince, J.L - Simultaneous Switching Ground Noise Calculation for Packaged CMOS Devices, IEEE Journal of Solid State Circuits, Vol 26, No 11, November 1991.

[13] Gabara, T, Thompson, D - Ground Bounce Control in CMOS Integrated Circuits, AT&T Bell Laboratories, Allentown, PA International Solid State Circuits Conference, 1988.